UNIVERSITY OF QUEENSLAND

Department of Mechanical Engineering

N86-15337

Unclas
03166

G3/20

(NASA-CR-176420) SCRAMJET SIDEWALL BURNING: PRELIMINARY SHOCK TUNNEL RESULTS (Queensland Univ.) 56 p HC A04/MF A01 CSCL 21H

SCRAMJET SIDEWALL BURNING - PRELIMINARY SHOCK TUNNEL RESULTS

NASA CONTRACT NO.NAGW-674

by

R.G. Morgan, A. Paull,
N. Morris and R.J. Stalker

Research Report No: 12/85

ABSTRACT

This report covers experiments performed with a two dimensional model scramjet with particular emphasis on the effect of fuel injection from a wall. Air flow with a nominal mach number of 3.5 and varied enthalpies was produced for these experiments using the shock tunnel T3 at the Australian National University. It was found that neither hydrogen injection angle nor combustor divergence angle had any appreciable effect on thrust values while increased combustor length appeared to increase thrust levels. Specific impulse was observed to peak when hydrogen was injected at an equivalence ratio of about 2. Lowering the mach number of the injected hydrogen at low equivalence ratios, less than 4, appeared to benefit specific impulse while hydrogen mach number had little effect at higher equivalence ratios. When a 1:1 mixture by volume of nitrogen and oxygen was used instead of air as a test gas, it was found that hydrogen combustion was enhanced but only at high enthalpies.

In other experiments, silane was centrally injected into flow conditions where hydrogen was found not to burn. In all cases, silane was observed to be most reactive. From heat transfer calculations it was concluded that the condition of the boundary layer was laminar but anomalies between observed and predicted heat transfers have yet to be fully explained. Temperature measurements showed also a significant wall cooling effect from high equivalence ratio injection of hydrogen from a reservoir at ambient temperature.

SCRAMJET SIDEWALL BURNING - PRELIMINARY SHOCK TUNNEL RESULTS

NASA CONTRACT NO. NAGW-674

R.G. Morgan

A. Paull

N. Morris

R.J. Stalker

CONTENTS

NOTATION

H_s	Stagnation enthalpy	MJ/kg
I	Injector location	
I_{sp}	Net specific impulse	sec
N_I	Intake Mach number	
M_J	Hydrogen jet Mach number	
NOX	Oxygen enriched air, 50% nitrogen, 50% oxygen by volume	
P	Local static pressure	kPa
P_I	Intake static pressure	kPa
P_s	Stagnation pressure	MPa
$\dot{q}$	Surface Heat transfer rate	W cm^{-2}
R_e	Freestream unit Reynolds number	m^{-1}
ST	Start of diverging section	
TH	Fuel on minus Fuel off thrust	N
T_I	Intake static temperature	K

T_W	Wall surface temperature rise	K
U_I	Air velocity at intake	Kms^{-1}
X	Wetted length measured from intake	mm
θ_D	Thrust surface divergence angle	degrees
θ_J	Fuel jet injection angle	degrees
ϕ	Equivalence ratio	
ΔP	$(P/P_I)_{Fuel\ on} - (P/P_I)_{Reference}$	

LIST OF FIGURES

21. Temperature profiles for constant area duct, NOX and air test gas, $\phi \sim 4.7$, $H_s = 6.1$ MJ/kg

22. Pressure profiles for constant area duct, NOX and air test gas, $\phi \sim 4.7$, $H_s = 6.1$ MJ/kg

23. Temperature profiles for constant area duct, NOX and air test gas, $\phi \sim 4.5$, $H_s = 4.2$ MJ/kg

24. Pressure profiles for constant area duct, NOX and air test gas, $\phi \sim 4.5$, $H_s = 4.2$ MJ/kg

25. Pressure profiles for constant area duct, $\phi \sim 1$, $H_s = 6.1, 4.2, 2.65$ MJ/kg

26. Pressure profiles for constant area duct, silane injection, $\phi \sim 1$, $H_s = 2.65$ MJ/kg

27. Pressure profiles for constant area duct, $M_I = 4.5$, hydrogen injection $\phi \sim 1$, $H_s = 1.9, 2.65, 3.43$ MJ/kg

28. Pressure profiles for constant area duct, $M_I = 4.5$, silane injection , $\phi \sim 1$, $H_s = 1.9$ MJ/kg

29. Pressure profiles for constant area duct, $M_I = 5$, silane injection, $\phi \sim 1$, $H_s = 4.2$ MJ/kg

30. Pressure profiles for constant area duct, $M_I = 5$, silane injection, $\phi \sim 1$, $H_s = 4.2$ MJ/kg

31. Pressure profiles for constant area duct, $M_I = 5$, silane injection, $\phi \sim 1$, $H_s = 8.7$ MJ/kg

32. Combustion chamber pressure/time, constant area duct, $M_I = 5$, $\phi \sim 1$, $H_s = 4.2, 6.1, 8.7$ MJ/kg

33. $\dot{q}$ profiles constant area duct without injector, $H_s = 2.65, 4.2, 6.1$ MJ/kg

34. $\dot{q}$ profiles constant area duct, wall injector, fuel off, $H_s = 4.2, 6.1, 8.7$ MJ/kg

35. $\dot{q}$ profiles 15° diverging duct, wall injector, fuel off, $H_s = 4.2, 6.1, 8.7$ MJ/kg

36. $\dot{q}$ profiles constant area duct, wall injection, $\phi = 0 - 9$, $H_s = 8.7$ MJ/kg

37. $\dot{q}$ profiles 15° diverging duct, wall injection, $\phi = 0 - 9.6$, $H_s = 8.7$ MJ/kg

SCRAMJET SIDEWALL BURNING - PRELIMINARY SHOCK TUNNEL RESULTS

NASA Contract No. NAGW-674

INTRODUCTION

This constitutes a progress report on Shock Tunnel Studies of Scramjet Phenomena. The work reported here was initiated in May,1985, as an extension to NASA Contract No. NAGW-674.

The purpose of the extension was primarily to allow work done under the contract to include studies of combustion in supersonic streams with hydrogen fuel injected supersonically at the sidewall. Experiments were planned to provide data over a wide range of fuel injection and combustion chamber conditions, with the intention of establishing trends and identifying parameters which are likely to be of importance. Simple two dimensional geometries are employed, with measurements of heat transfer and surface pressure distributions.

The experiments were designed to allow variation of the following parameters:

(a) Angle at which hydrogen is injected with respect to the surface.

(b) The Equivalence Ratio and the Mach number of the hydrogen at injection,

(c) The combustor divergence,

(d) The combustor length,

(e) The stagnation enthalpy of the airflow. In view of the large number of parameters which were varied, this was for the most part limited to three values, namely, 4.2, 6.1 and 8.7 MJ/kg, corresponding to flight speeds of 2.9, 3.5 and 4.2 km s^{-1} respectively.

Other experiments were performed to investigate the following topics:

(f) The freestream oxygen concentration

(g) Silane injection

(h) Heat transfer

(i) Cooling effect of hydrogen injection from the wall.

EXPERIMENTAL APPARATUS

The experimental apparatus is shown schematically in Figure 1. It is a two dimensional model, with a width of 51 mm. The hydrogen was injected at the downstream face of a step, which spanned the full width of the duct. the model was constructed to follow, as closely as possible, the dimensions of a previous model with a central injection strut. Thus the injection step was located at the same distance from the intake as the trailing edge of the central injection strut, and the height of the step was identical with the thickness of the strut. This was done in order to allow realistic comparisons between the two geometries. The step was followed by a parallel section, which was 25 mm in length, leading to a straight thrust surface of variable divergence angle. The configuration with divergence angle set to 0° is subsequently referred to as a constant area duct, because downstream of the injector step there is no further change in the duct's cross sectional area. The hydrogen was injected downstream from behind a 5 mm step in the wall. The construction of the injector is shown in Figure 2. It provides for injection at angles of 7½ and 15° to the flow and the throat size can be set at 0.3, 0.9 or 1.6 mm. The Mach number of the hydrogen jet is estimated by assuming isentropic expansion from the hydrogen plenum chamber conditions, measured at point X on Figure 2, to the duct intake pressure. The supply pressure for a given Mach number is therefore predetermined, and the equivalence ratio is set by the

area at the throat. The injection system was designed for a maximum operating pressure of 10 MPa, and the injection conditions that can be achieved are summarized in Figure 3.

Hydrogen injection mass flows were calibrated by following the variation of hydrogen injection pressure during a test, and relating this to the fall in pressure in the hydrogen reservoir.

The thrust surface was instrumented with pressure transducers, and/or thin film heat transfer gauges, and model intake conditions were monitored by two static pressure transducers.

Throughout this report, whenever possible, heat transfer measurements are presented, calculated from the surface temperature measurements. However, when the temperature rise is small due to the cooling effect of injecting hydrogen, the heat transfer measurements become very noisy and difficult to interpret. Hence, for these conditions surface temperature measurements are used directly for comparisons between different experiments. While it is understood that at any point in time after the onset of heating the temperature rise is proportional to the heat transfer rate only if that rate is constant, it may still be used for qualitative comparisons.

Contoured nozzles were used to supply shock heated air from the shock tunnel to the model intake. The test conditions were monitored by shock speed measurements in the shock tube, coupled with measurements of the pressure at the downstream end of the shock tube adjacent to the entrance to the nozzle. Flow conditions at the intake to the model are summarized in Table 1.

Test conditions were reasonably reproducible. However variations in results obtained for nominally identical test conditions did occur. In an attempt to suppress these variations the pressures measured were normalized by dividing by the intake pressure, whenever reasonable intake pressure measurements were

available. Normalizing the thrust on the thrust surface with respect to the intake pressure also provided a means of determining when a flow with a constant air flow Mach number occurred. It was assumed that the air flow Mach number was steady if the normalized thrust was steady.

(a) INJECTION ANGLE

The hydrogen was injected downstream, parallel to, and at 15° to the horizontal into the freestream using a 0.9 mm throat. Preliminary measurements of the mass flow rates of the two injectors, confirm the rates to be similar.

Figure 4 displays the pressures measured on the constant area duct normalized with respect to the intake pressures, when hydrogen is injected at an equivalence ratio of 8.8 into a freestream of stagnation enthalpy of 8.7 MJ/kg. It can be seen that no significant change is observed between the traces obtained for the different injections. Figure 5 shows the increase in temperature measured under the same conditions. It is seen that a consistently lower temperature is observed when injecting at 15°. When the test conditions were changed a different pressure trend was noted. These results are shown in Figure 6, and display the pressures measured on a 7° divergent duct when hydrogen is injected at an equivalence ratio of 1.5 into a freestream of stagnation enthalpy of 61 MJ/kg. It is seen at this enthalpy an increase in thrust was associated with the 15° injector, although it should be noted that at this equivalence ratio combustion is marginal.

In conclusion, the mechanism by which the injection angle alters the development of thrust and cooling of the thrust surface is not understood. It would appear that a significant increase in cooling has occurred with the 15° injector. However results are inconclusive as regards the pressure distribution for different injection angles. This does not necessarily mean that increased mixing did not occur, because it is possible that the observed extra cooling with 15° injection may have expanded the quenching layer discussed in Section B.

It is possible that if heated hydrogen was used the pressure profiles would be more sensitive to injection angle.

(b) EFFECT OF MACH NUMBER AND EQUIVALENCE RATIO

Due to the limited range of injector throat sizes it was not possible to cover the full range of Mach number at all equivalence ratios, as may be seen from Figure 3. For instance, at the maximum injection Mach number of 3.2, the lowest equivalence ratio possible was 7.3 with a 0.3 mm throat. However, the situation improves at lower Mach number, so that for a Mach number of 2.6 equivalence ratios between 10 and 3 are possible. Consequently, the data presented here are more comprehensive in the lower Mach number regions.

The scramjet was configured with the thrust surface inclined at 15° and the hydrogen was injected parallel to the intake flow. The thrusts used to calculate specific impulse were obtained by linear interpolation between pressure monitoring points, and were taken during the steady flow period.

In Figure 7A specific impulse is plotted against jet Mach number for the full range of equivalence ratios and enthalpies used.

There is seen to be a consistent reduction of specific impulse with Mach number up to a Mach number of about 2.5. The hydrogen is injected at a lower velocity than the air, so that an increase in hydrogen Mach number reduces the velocity difference across the mixing layer, and might be expected to reduce the amount of mixing and combustion. The lower temperatures associated with the higher Mach numbers might also have a quenching effect on the flame.

The same data is also displayed in Figures 7B to 7D for equivalence ratio ranges of 1-2, 1-3.5 and 3.5-11, in order to decouple the effects of ϕ and M_J as far as is possible. It can be seen that it is the lower values of equivalence ratio which have the strongest Mach number dependence. Figure 7D shows that the specific impulse shows no systematic Mach number dependence at the higher equivalence ratios. This effect is confirmed in Figure 8 where the

pressure against distance profiles are shown for a stagnation enthalpy of 8.7 MJ/kg with an equivalence ratio of 8 and injection Mach numbers of 3.1 and 2.34.

There is not sufficient data at present to cover the effects of Mach numbers below 2.3 on high equivalence ratios. In Figure 9 the pressure against distance profiles are shown for $\phi \sim 2$ and jet Mach numbers of 1.63 and 2.37. It is seen that the increased thrust at low Mach numbers is achieved in the region immediately downstream of the expansion corner.

Wall injection is found to give smaller values of specific impulse than was achieved with the central injector, and the experimental accuracy is correspondingly reduced. Error bars have therefore been included in Figure 7 to show what is considered to be the appropriate error.

The effect of injection Mach number was also studied in respect to the heat transfer rates. The gauges were positioned where the fuel or heating rates begin to rise towards the fuel off values as the effects of mixing and combustion offset the cooling effect of unburned fuel. This region was expected to be most sensitive to the effects of Mach number on mixing. In Figure 11 the surface temperatures are shown for an equivalence ratio of 4.4, jet Mach numbers of 2.8 and 2.2 and stagnation enthalpy of 8.7 MJ/kg. No significant difference can be seen between the two cases, which suggests that the cooling effect is a function only of the total amount of hydrogen injected, and is Mach number independent in this range. This supports the previous conclusion based on pressure measurements for this equivalence ratio range.

The tentative conclusion of this section is that specific impulse reduces with increasing Mach number, but this effect would be partially offset by the increased kinetic energy of the injected hydrogen itself. Because the specific

impulse is so low, substantial changes must be made to improve combustion with wall injection, and the Mach number dependence will not necessarily apply to a modified geometry.

In Figure 10 the net thrust, defined as the fuel on thrusts minus the fuel off thrusts, is plotted against equivalence ratio. The large amount of scatter is due in part to the range of Mach number achieved at a given value of ϕ. The overall trend is that there is no significant increase in combustion above an equivalence ratio of about 2, and very little combustion at equivalence ratios of less than 1.5.

To further understand the effect of equivalence ratio, a series of experiments was done with the constant area duct. Measurements from tests without injection of hydrogen displayed large axial pressure gradients. These disturbances arise from compressions and expansions generated by the separation and subsequent reattachment of the flow as it passes the injection step. They may also be produced by surface protuberances at adjoining sections of the model surface downstream of the injector. These effects were not significant when the model was set with a diverging thrust surface, but in the constant area configuration multiple reflections across the duct produced non-uniform, but repeatable, pressure profiles. When hydrogen was injected at equivalence ratios above 2 these large pressure gradients disappeared. This effect is not attributable to combustion because, as it seen in Figure 12, hydrogen injection into a flow of nitrogen at the same conditions produced a steady pressure level throughout the duct. Therefore, for the following section the fuel on results for air were compared with the fuel on pressures for nitrogen, rather than the fuel off case for air. This made the pressure traces smoother and easier to interpret, and was also felt to give the best indication of combustion by eliminating inherent gas dynamic effects induced by the model geometry which were not present during fuel injection.

In Figure 13 the difference is shown between the normalized pressures measured for equivalence ratios of 1.3, 2.6 and 8.5 and the normalized pressures when the hydrogen was injected into a nitrogen test gas at a pressure that would be equivalent to an equivalence ratio of 2.6 for air.

It is seen that increasing equivalence ratio produces no significant increase in pressure, and hence combustion, for equivalence ratios above 2.6. Very little pressure rise was observed at an equivalence ratio of 1.3 in Figure 13. By comparing Figures 12 and 13 it can be seen that at the equivalence ratio of 1.3 the pressure rise and distribution is similar to that of the fuel off case, and that no significant combustion has occurred. However, at an equivalence ratio of 2.6 there is a large pressure rise and it appears that the onset of combustion occurs within a small range of equivalence ratio. At the lower equivalence ratios the hydrogen jet is thinner and therefore the combustion zone is closer to the wall and subjected to increased heat losses,and this may explain the sudden onset of ignition with increasing equivalence ratio. This quenching mechanism does not exist with central injection, and indeed previous work with central injection indicated that no lower limit on equivalence ratio exists below which combustion cannot occur.

The results of Figure 13 are consistent with the data presented in Figure 10 for net thrust against equivalence ratio with a thrust surface divergence of 15°. Both the constant area and the diverging ducts indicate that there is a layer of hydrogen close to the wall which cannot be made to burn even when mixed with oxygen from the freestream flow, due to quenching effects. The hydrogen contained in this region appears to correspond to an equivalence ratio of about 1.3, since no combustion was observed when less hydrogen was injected. As more hydrogen is injected a combustion region is created away from this quenching zone, and pressure rises were observed. When equivalence ratios were

increased above 2.5 no further pressure rise could be induced in the constant area duct. At this point the amount of hydrogen contained in the region clear of the quenching zone would produce an equivalence ratio of approximately 1, and if fully burned it would consume all the oxygen entering the duct. This indicates that the amount of hydrogen which is unburned due to wall cooling effects does not change much with injection pressure, and it also explains why no further combustion occurs above equivalence ratios of 2.5.

It is is assumed that the amount of hydrogen unburned due to quenching effects is constant, then it is possible to redefine equivalence ratio and specific impulse based on the unquenched hydrogen injection rate. Whilst this does not represent a true measure of performance, it does provide a useful comparison between the combustion and thrust producing mechanisms for wall and central injection. In this way the performance reduction due to quenching, which might not occur on a flight vehicle with heated fuel and hot walls, may be eliminated from comparisons between the two injectors.

In Figure 14a and 14b for enthalpies of 4.2 and 8.7 MJ/kg respectively, the specific impulse is shown for equivalence ratios calculated with and without the quenched hydrogen component. Also shown are the specific impulses achieved with the central injector. It is noted that when compared on this basis the two injection mechanisms give comparable performance. This is despite the fact that combustion regions near the wall do not contribute to thrust on being expanded around the corner, as discussed in Section (c). It therefore appears that the wall injector has the same potential as the central strut, provided wall quenching problems can be overcome.

(c) THE EFFECT OF COMBUSTOR DIVERGENCE

In Figure 15 the specific impulse/divergence relationship is shown for the three different enthalpies for an equivalence ratio of about 2.5. Also shown on the figure are the results from an earlier series of experiments with a central injector. It is noted that there is not significant variation of performance with divergence angle, and that wall injection gives much less thrust than the central injector.

In Figure 16 the pressure against distance dependence is shown for both wall and central injection. Two separate mechanisms are evident for thrust production with the central injector. Firstly, pressure waves from the combustion region act on the surface to increase the pressure, and hence the thrust, over the fuel off condition. Secondly, combustion leads to a region of low Mach number which interacts with the expansion fan from the start of the diverging section to produce compression waves which increase the pressure on the thrust surface.

However, for the wall injector the situation is different, leading to an increasing Mach number moving away from the wall. The expansion originates in the low Mach number region near the wall, which leads to a higher pressure immediately downstream of the corner than is obtained for the fuel off condition. As the expansion propagates into the higher Mach number region, expansion waves are generated which propagate back to the thrust surface to equalize the pressures between the freestream and the wall. In the region between the corner and the re-establishment of the freestream, pressure level, the increased surface pressure leads to an increment in thrust. For the conditions presented in this section the divergence is started only a small distance downstream of injection. This means that the low Mach number region does not spread far from the wall and the region of increased pressure on the

thrust surface is small. This mechanism does not therefore contribute significantly to thrust production in this case. All the thrust is obtained by means of the first mechanism mentioned above. This effect partially explains the reduced thrust obtained by wall injection. For both configurations the diverging section was started 25 mm downstream of the injection station. This means that for wall injection the combustion region is expanded after only 25 mm of development. However, for the central injector the combustion zone is unaffected until the expansion fan from the corner has propagated to the centre line, thus allowing approximately 25 mm extra for mixing and combustion. This extra combustion region before the jet is expanded could be a cause of significant thrust increment when the combustion chamber is short.

Other contributory factors are likely to be the loss of heat from the combustion zone to the wall, and the fact that there is only one hydrogen/air mixing layer, compared to two for the central injector.

(d) THE EFFECT OF COMBUSTOR LENGTH

A short series of tests was performed with an extension of 150 mm fitted to the constant area section before the start of divergence. This allows the combustion region to spread further into the flow before being expanded, and should enable more thrust to be achieved by the second mechanism mentioned above. The specific impulse for this case is also shown on Figure 15 for 15° divergence. Significantly higher specific impulse is achieved, although it is still less than would be obtained with a central injector. In Figure 17 the pressure/distance dependence is shown for equivalence ratios of 3 and 1.4. It is again seen that combustion did not occur at the lower value of equivalence ratio. The shape of the curves is characteristic of the second mechanism of thrust production, with a large ΔP immediately after the expansion, followed by a gradual decay to fuel off levels. This illustrates the potential of the expansion/jet interaction mechanism to generate thrust in the wall injection configuration.

(e) EFFECT OF THE STAGNATION ENTHALPY OF THE AIRFLOW

Inspection of the data presented in Figure 7a for specific impulse against Mach number shows no significant enthalpy dependence for the range of conditions presented. This is also illustrated in Figure 10 for the results of TH against ϕ. Similarly, within the range of experimental accuracy, no enthalpy dependence could be observed in Figure 15 for the variation of specific impulse with thrust surface divergence.

This apparent insensitivity to enthalpy is possibly caused because the beginning of the thrust surface is located only 25 mm from the injector, which is insufficient for significant combustion.

When tests were performed for a constant area duct, a significant enthalpy effect was observed,as shown in Figure 18. Combustion occurs after injection with a delay period which decreases with the higher static temperatures asscciated with the higher energy flows. This is consistent with small ignition delay and reaction times at high static temperatures.

It was noticed that higher pressure rises were not achieved with the low enthalpy tests, despite the fact that the nearly steady pressure levels suggest that no more combustion was taking place. This is contrary to expectations, and to observations with a central injector, and may provisionally be attributed to an increase in the size of the quenched zone attached to the wall at the lower temperatures.

(f) EFFECT OF OXYGEN ENRICHMENT OF FREESTREAM AIR FLOW

A 50% mixture by volume of nitrogen and oxygen was used as a test gas to gauge the effect of freestream oxygen concentration. Figures 19, 21 and 23 show the increase in temperature above ambient temperature, observed in a constant area duct for an air and oxygen test gas at stagnation enthalpies of 8.7, 6.1 and 4.2 MJ/kg respectively. Figures 20, 22, and 24 display pressures in the duct, normalized with respect to the intake pressure, for the samee enthalpies and test gases. The constant area duct configuration did not allow measurements to be obtained at a distance less than 42 mm downstream of the injector which is unfortunate, for as seen in Figures 20 and 22, a significant amount of combustion occurred in this region when injecting into the enriched test gas. However, the measurements obtained were sufficient to display the difference in combustion rates between an air test gas and an enriched test gas. Upon completion of these experiments a fault was detected in the calibration of the pressure measurements. However, although the quantitative values of pressure may be in doubt, it is believed that the data is useful for qualitative comparison between runs within this set of experiments. The hydrogen injection pressure was monitored at approximately 2800 kPa which corresponds to equivalence ratios of 5.5 to 4.3 for air, and 2.2 to 1.7 for the enriched mixture. Injection was through the 15° injector into the oxygen enriched test gas and through the parallel wall injector into the air test gas. For air at 8.7 MJ/kg both parallel and 15° injection were used. Both injectors had a throat size of 0.9 mm.

For the following data on a constant area duct, it is assumed that invariance of pressure with downstream distance establishment of steady pressures indicates that combustion is complete. However, it is noted in section (b) that this does not necessarily mean that either all the hydrogen or all the oxygen has been burnt.

Oxygen enrichment was found to strongly affect combustion, but to an extent which was a function of temperature. Figure 19 shows that at the higher enthalpy the surface temperature rises were greater when the oxygen enriched test gas was used. This is taken to indicate an increase in combustion. This increase in burning is also reflected in Figure 20 where it is seen that the pressures for the oxygen enriched test gas are greater. It was also noted that when injecting into the enriched gas the rise to a constant pressure level was achieved approximately 2½ times faster than when injected into air. It is interesting to note the concentration of the oxygen in the enriched gas is also approximately 2½ times that of air.

At an enthalpy of 6.1 MJ/kg it is seen in Figure 21 that the temperatures measured for the two test gases are approximately the same. It can be seen in Figure 22 that the values of the steady level pressures are also the same. However, this level is reached further upstream with the enriched test gas. In addition, Figure 22 indicates that the heat is released earlier with the higher oxygen content, but it is seen in Figure 21 the total amount released is unchanged.

At an enthalpy of 4.2 MJ/kg it is seen in Figure 25 that a slight, but consistent reduction in the pressures exists for the enriched test gas. This is consistent with, but could not fully explain the decrease in temperatures recorded for the enriched test gas as displayed in Figure 23.

Two effects have been observed at the higher enthalpies. An increase in combustion rate, as indicated by the rapid increases in pressures along the duct, and an increase in the total amount of heat released as indicated by the steady pressure levels downstream in the duct. The first effect is only apparent at the higher enthalpies. This is probably because at the higher enthalpies, ignition delay times are small and the increased mixing leads to

a rapid increase in combustion. It is not understood why this second effect is also only apparent at higher enthalpies, because the observed increase in the mixing rate, coupled with previous results which indicate that at these equivalence ratios there is sufficient unquenched hydrogen to support extra burning, should produce an increase in combustion.

(g) SILANE COMBUSTION

For these experiments, the model was configured as a constant area duct. Silane mixed with hydrogen in the ratio 20% to 80% by volume was centrally injected at equivalence ratios of order one, into air flow conditions where hydrogen alone was observed to burn with only marginal pressure rise, or not to burn at all. Equivalence ratios were based on total fuel injected, and included the components of both hydrogen and silane.

Cases were limited to those where failure of hydrogen combustion could be attributed to either a dominant low temperature effect or a dominant low pressure effect. In all cases, the silane mixture was observed to burn vigorously.

Low Temperature Combustion of Silane

A silane mixture was centrally injected into two flow conditions of Mach 3.5 and Mach 4.5 where hydrogen would not ignite due to low temperatures.

Firstly, the combustion temperature limit of hydrogen was determined at Mach 3.5 by decreasing flow enthalpies until hydrogen ignition stopped occurring. By decreasing flow enthalpies, the model intake temperature is reduced, while the intake pressure remains approximately constant. In Figure 25 the local static pressures, normalized by nozzle stagnation pressure is plotted against distance along the duct for different flow enthalpies. It was seen that combustion occurs at an enthalpy of 4.2 MJ/kg, but not at 2.65 MJ/kg. Therefore the ignition limit for these conditions lies at intake static temperatures of between 700K and 1100K.

Air at the enthalpy of 2.65 MJ/kg was shown not to support hydrogen combustion when expanded to Mach 3.5. This corresponded to an intake temperature of 700K and intake pressure of 120 kPa. It was at this condition that silane was injected and as seen from a plot of duct pressures normalized by nozzle stagnation pressure against distance (Figure 26), the silane burnt vigorously while hydrogen remained unreactive.

Flows at Mach 4.5 which correspond to lower intake pressures were then considered. These were produced by using a Mach 5 contoured nozzle and a model intake attachment which compressed the flow to Mach 4.5 using two plates inclined at 2.57°. The intake attachment was configured such that the shocks created by the flat plates did not enter the intake of the constant area duct.

As for the Mach 3.5 case, temperature limits were determined for hydrogen combustion by decreasing flow enthalpy until hydrogen did not ignite, as shown in Figure 27. An interesting outcome of this exercise was that a lower combustion temperature limit for hydrogen was observed for the higher Mach number of 4.5 despite the lower pressures. This may be seen by comparing Figures 25 and 27. This effect might be attributed to the enhanced boundary heating in hypersonic flows which could cause hydrogen ignition in otherwise unfavourable low pressure conditions.

Air at an enthalpy of 1.90 MJ/kg and Mach number of 4.5 was found not to support hydrogen combustion. This corresponds to an intake temperature of 370K and pressure of 30 kPa. When silane was injected, combustion was again observed while hydrogen remained essentially unreactive, see Figure 28.

Low Pressure Combustion of Silane

Air with enthalpies of 4.2, 6.1 and 8.7 MJ/kg was expanded to Mach 5 which produced low pressure flows where the combustion of hydrogen was marginal over a wide temperature range.

At these conditions, however, silane burns readily. This is shown in Figures 29, 30, 31, which are plots of absolute pressure versus distance along the duct at comparable points in test time.

It is noted that pressure rises due to silane combustion decrease with an increase in flow enthalpy. This is consistent with the expectation of heat release at higher temperatures giving a smaller relative pressure rise. This trend is confirmed in a plot of pressure averaged over the thrust surface, against test time, showing consistent difference between the pressures at the three enthalpies. (Figure 32)

(h) 'EAT TRANSFER MEASUREMENT - BOUNDARY LAYER PREDICITION

Measured fuel off heat transfer rates at comparable points in run time are compared with empirical predictions for the three cases of the model configured as a constant area duct, with and without a wall injector and with the thrust surface inclined at 15°. These experiments were carried out at an intake Mach number of 3.5 and enthalpies of 2.65, 4.2, 6.1, 8.7 MJ/kg.

Heat transfer rates were calculated from the surface temperature time history using a one-dimensional, semi-infinite solution to the unsteady internal conduction of heat within the substrate. The stored temperature signal was then analysed digitally, to a technique presented in Schultz and Jones[1], in order to calculate the heat transfer rates.

Empirical predictions were obtained following the treatment presented by Stollery and Coleman[2] for a turbulent boundary layer and flat plate. This is based on an empirical method by Eckert[3] whereby the heat transfer rate may be estimated from a knowledge of freestream conditions and the local wall static pressure.

For a laminar boundary layer, heating rates were estimated using an empirical correlation from Hayes and Probstein[4].

For both cases, the conditions on the edge of the boundary layer were calculated by assuming isentropic flow from the inlet conditions to the local static pressure.

Turbulent heat transfer rates calculated empirically were found to be of order ten times larger than the experimental values for all of the model configurations and so are not considered here on.

When the model is configured as a constant area duct without the injector fitted, experimental values of heat transfer correspond fairly well with the predicted laminar values. It is noted, however, that as the flow enthalpy is increased from 2.65 to 4.2 then 6.1 MJ/kg, the measured heat transfer rate tends to drop relative to the prediced values. See Figures 33(a), 33(b), 33(c) which show plots of experimental and predicted heat transfer rates against distance along the duct.

The wall injector was then fitted for comparison of results. For flow enthalpies of 4.2 and 6.1 MJ/kg, it is observed that the presence of the expansion and subsequent recompression caused by the 5 mm downward step has little effect on measured heat transfer rates compared to the case where the injector is not fitted (compare Figure 33 (b) with 34(a) and Figure 33(c) with 34(b)). This would indicate that the presence of the step has no significant effect on the condition of the boundary layer at the Reynolds number considered here. For the higher flow enthalpy of 8.7 MJ/kg (Figure 34(c)) it can be seen that the measured heat transfer rates depart significantly from the predicted values which supports the trend described for the previous configuration of measured heat transfer rate dropping relative to laminar predicted values with increasing flow enthalpy.

When the model thrust surface is inclined at 15°, the measured heat transfer rate is observed to depart significantly below predicted laminar values. This occurred even for the enthalpy of 4.2 MJ/kg (Figure 35(a)), where predicted and measured values for the non-inclined cases showed good agreement. As with the constant area duct, when the enthalpy is increased to 6.1 and 8.7 MJ/kg, the measured heat transfer rates depart further from the predicted laminar values. (Figures 35(b), 35(c))

It is concluded that the condition of the boundary layer appears to be laminar for all configurations considered here. However the empirical correlations used show only limited agreement with experimental values. For the constant area duct, flows at enthalpies greater than 6.1 MJ/kg give results which depart significantly from predicted values.

A significant increase in departure from theory with increase in flow enthalpy is also observed by East, Stalker and Baird[5]. It was shown however that if empirical correlations are calculated using a reduced frozen recovery enthalpy, rather than total enthalpy, greater agreement with experimental values result. Energy absorption through dissociation of test gases might explain then the reduced heat transfer rates compared with predicted values observed in these cases. The extent of the departure from predicted results for these experiments however appears to more than those presented by East, Stalker and Baird and at lower enthalpies, and so warrants more investigation.

When the surface is inclined at 15°, there appears to be little agreement at all with the empirical calculations for all enthalpies considered. This is despite the fact that in previous experiments by Morgan and Stalker [6] using a central injector and a conical Mach 3.5 nozzle at higher enthalpies than those considered above, twin thrust surfaces inclined at 7.5° gave experimental results about the same, or above, laminar predicted values. This discrepancy in results could be due to an increased divergence angle in this case.

As the test section in which the model is set is evacuated before operation, the hydrogen plenum chamber would tend to suck air back through the injector during a run until pressure is equalized. It has been estimated that sucking would occur for about 500 μs, which is a significant part of the steady test time. For the central injector this is not expected to influence the wall

boundary layer, but with a wall injector it will be removing gas from the region of separated flow which is likely to have a strong effect on the separation and reattachment process, and might influence the subsequent downstream development of the boundary layer.

As previously noted, the presence of the injector in the constant area duct had no appreciable effects on heat transfer rates. However, as the diverging section starts in close proximity to the injector, divergence coupled with effect described above, might effect heating rates.

(i) FILM COOLING EFFECT OF HYDROGEN

An outcome of the injection of hydrogen from the wall is a reduction of the local heat transfer rates. The effect of this is summarized in Figures 36 and 37 at an enthalpy of 8.7 MJ/kg for a constant area duct and a 15° diverging duct respectively.

Hydrogen injection is seen to produce a significant reduction in the heating rate. The cooling effect increases with equivalence ratio, as would be expected. The heating rate rises to the fuel off levels within a distance that increases with equivalence ratio, and is longer for 15° divergence than the constant area duct. This is consistent with the greater combustion heat release observed for the constant area duct.

There are two important differences between the experimental conditions reported here and a flight situation which should be noted. Firstly the cold wall produces a quenched zone which separates the burning gases from the wall. The increased wall temperatures of a flight vehicle would be expected to reduce the size of the quenched zone and correspondingly increase the heating rates. Secondly the hydrogen was supplied from a room temperature reservoir, whilst heated hydrogen is expected to be used on a full scale scramjet.

REFERENCES

1. D.L. Shultz and T.V. Jones, "Heat Transfer Measurements". Agardograph No.165, 1973.

2. J.L. Stollery and G.T. Coleman, "A Correlation Between Pressure and Heat Transfer Distributions at Supersonic and Hypersonic Speeds". Aeronautical Quarterly, Vol.26, pp.304-315, 1975.

3. E.R.G. Eckert, "Engineering Relations for Skin Friction and Heat Transfer to Surfaces in High Velocity Flow". Journal of the Aeronautical Sciences, Vol.22, pp.585, 1955.

4. W.D. Hayes and R.F. Probstein, "Hypersonic Flow Theory". Academic Press, New York and London, 1959.

5. R.A. East, R.J. Stalker, and J.P. Baird, "Laminar Flat Plate Heat Transfer Measurements from a Dissociated High Enthalpy Hypersonic Air Flow". Department of Aeronautics and Astronautics, Southampton University, Report No.338, 1977.

6. R.G. Morgan and R.J. Stalker, "Shock Tunnel Measurements of Heat Transfer in a Model Scramjet". Paper AIAA-83-6908 presented at AIAA 20th Thermophysics Conference, Williamsburg Virginia, 1985.

TABLE OF TEST CONDITIONS

H_s MJ/kg	M_I	T_I K	P_I kPa
8.7	3.5	2500	160
8.7	4.5	1740	32
8.7	5.0	1500	20
6.1	3.5	1700	160
6.1	4.5	1200	32
6.1	5.0	1000	20
4.2	3.5	1100	160
4.2	4.6	750	32
4.2	5.0	650	20
3.43	4.5	625	30
2.65	3.5	700	120
1.9	4.5	400	30

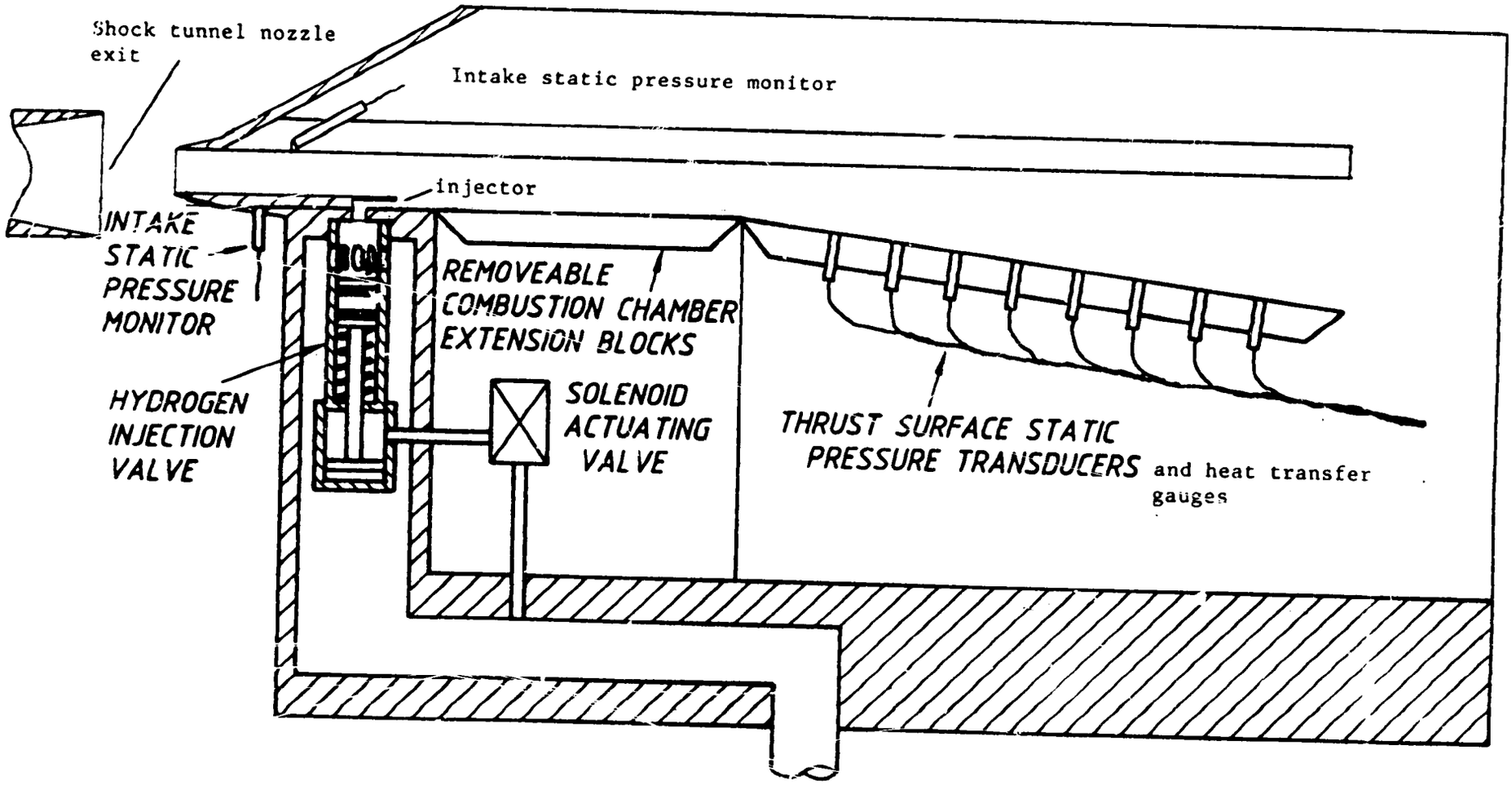

Fig 1. Schematic Diagram of Experimental Apparatus

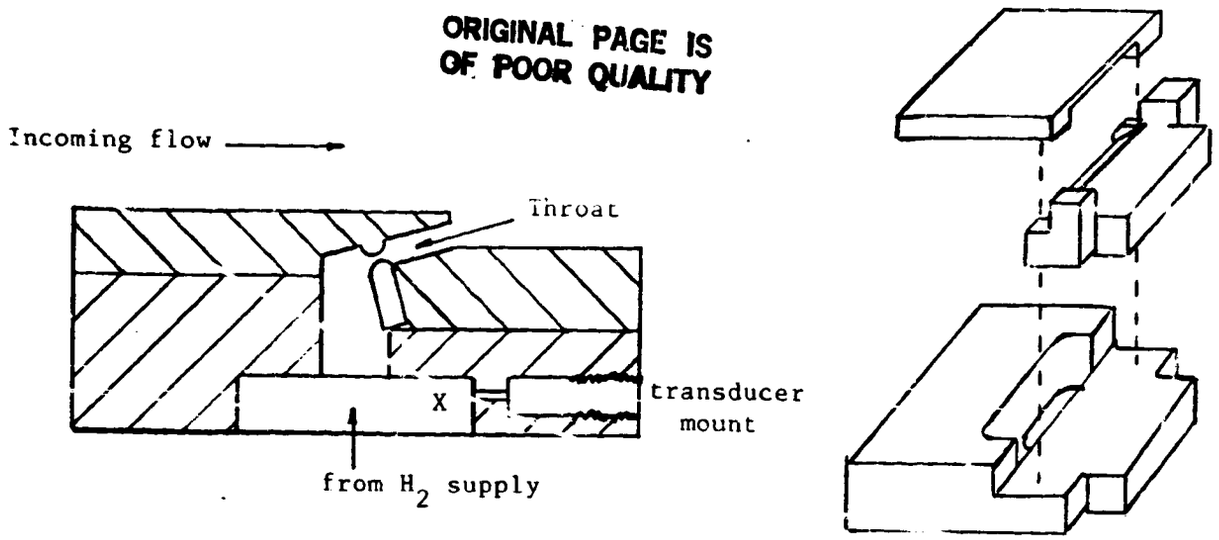

FIG.2 Wall Injector Schematic

8.7 MJ/kg

6.1 MJ/kg

4.2 MJ/kg

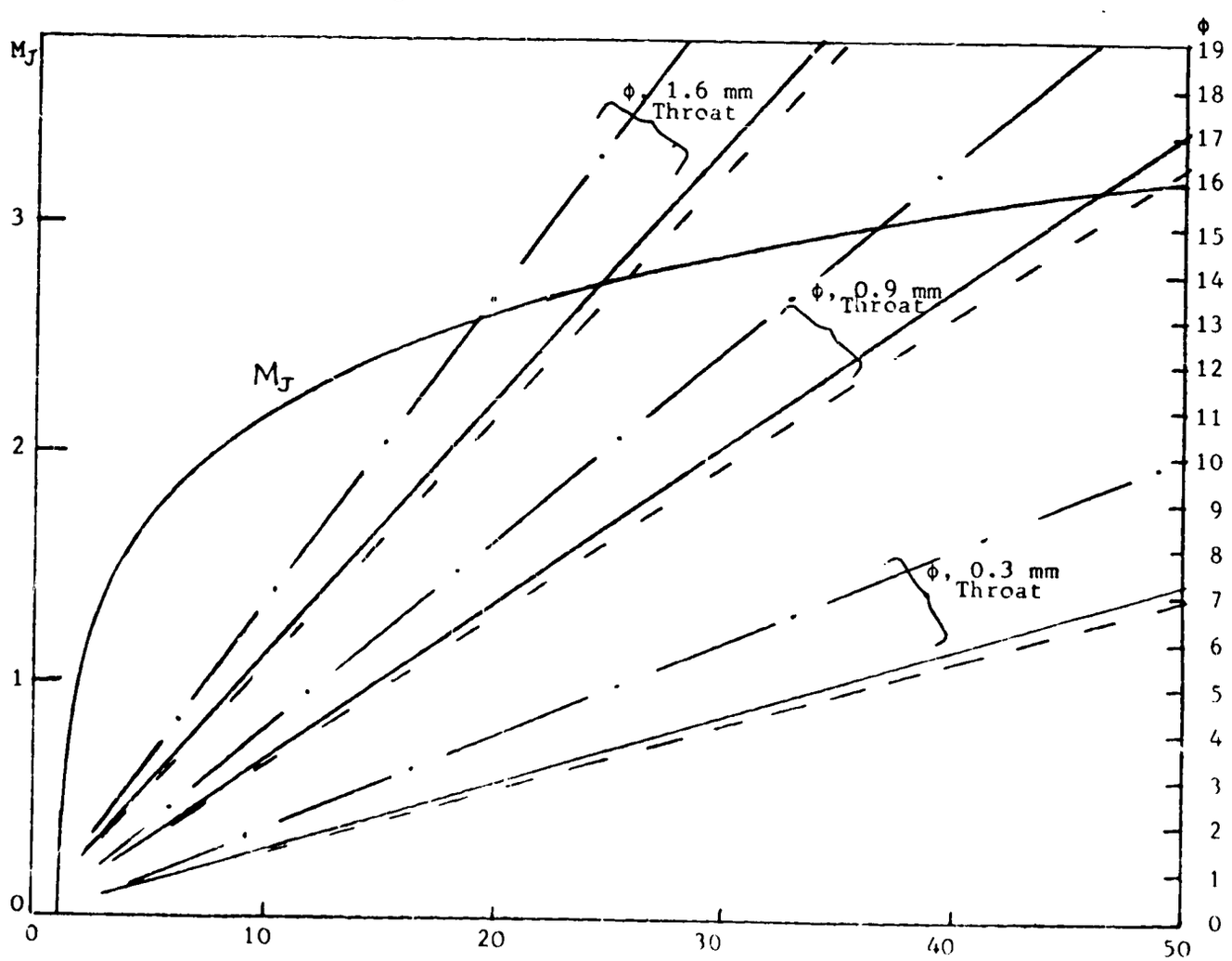

FIG. 3 Hydrogen Injection conditions

P/P_I

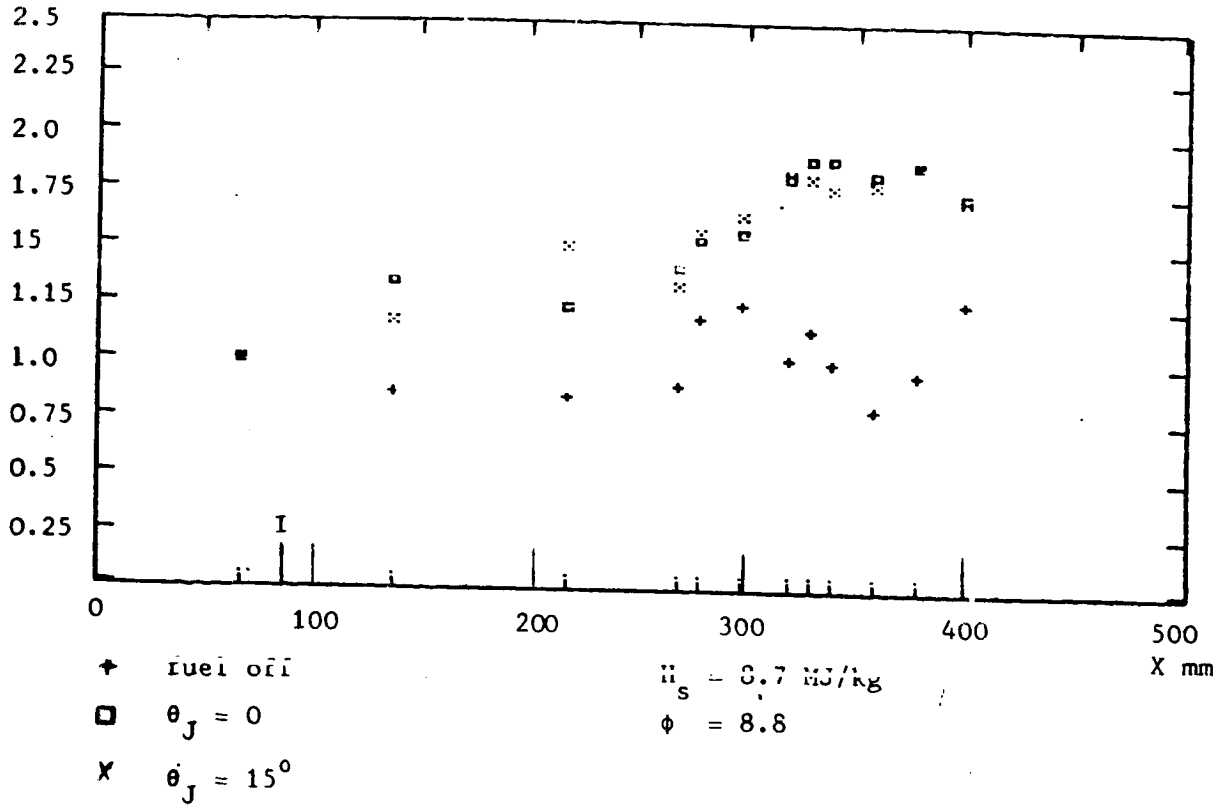

FIG. 4 Pressure profiles for different injection angles into a constant area duct

T_S K

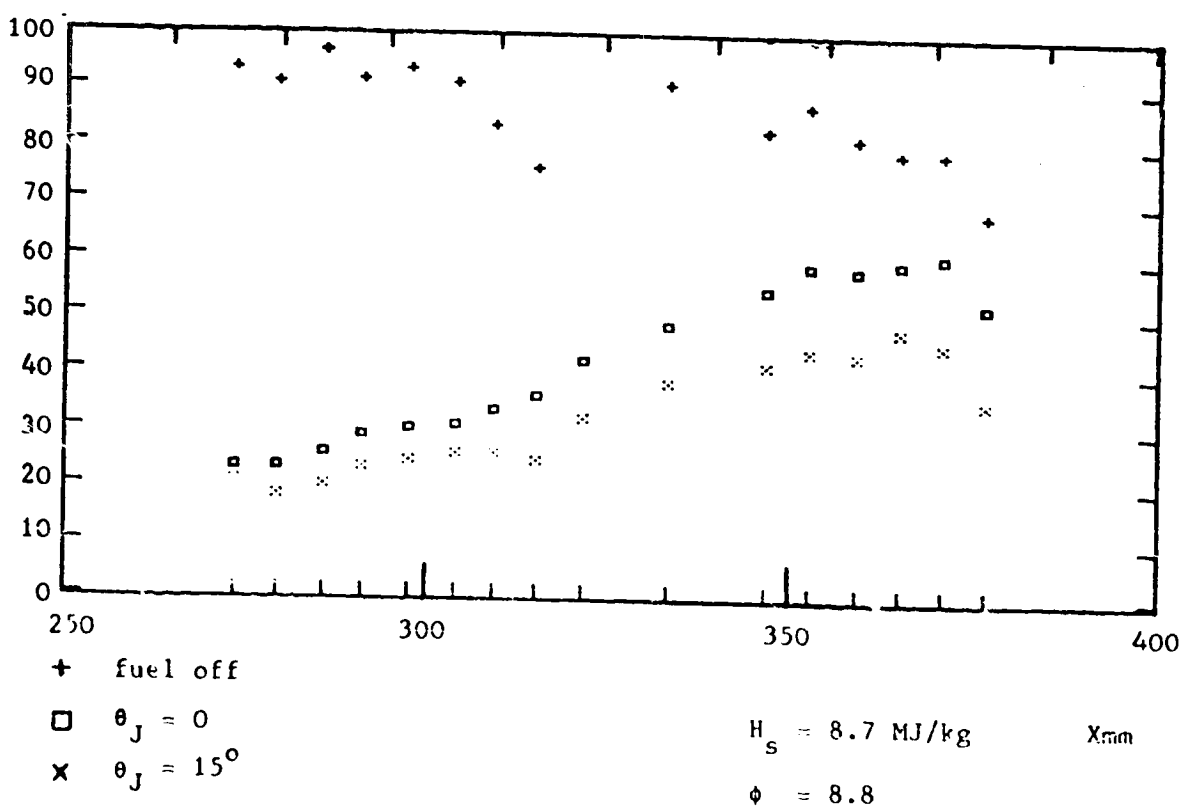

FIG. 5 Temperature profiles for different injection angles into a constant area duct.

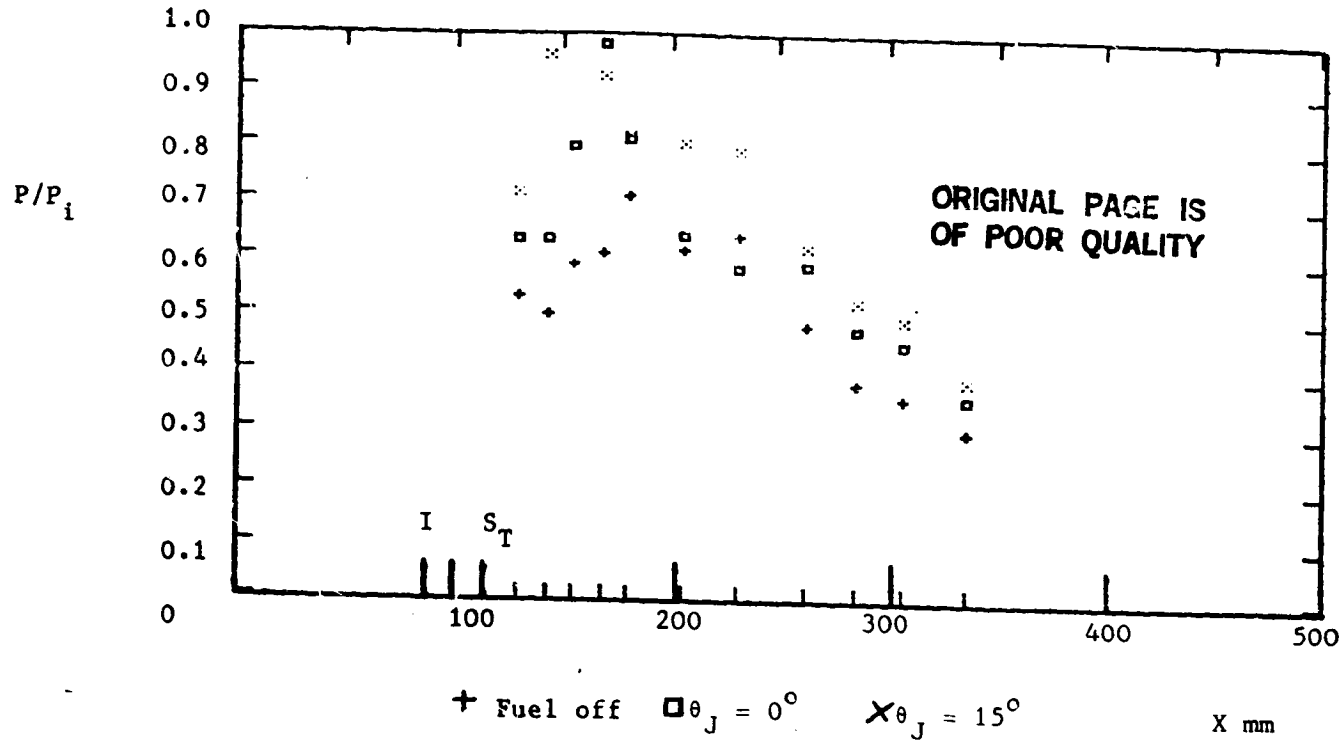

FIG. 6 Pressure profiles for a constant area duct at different injection angles H_s = 8.7 MJ/kg

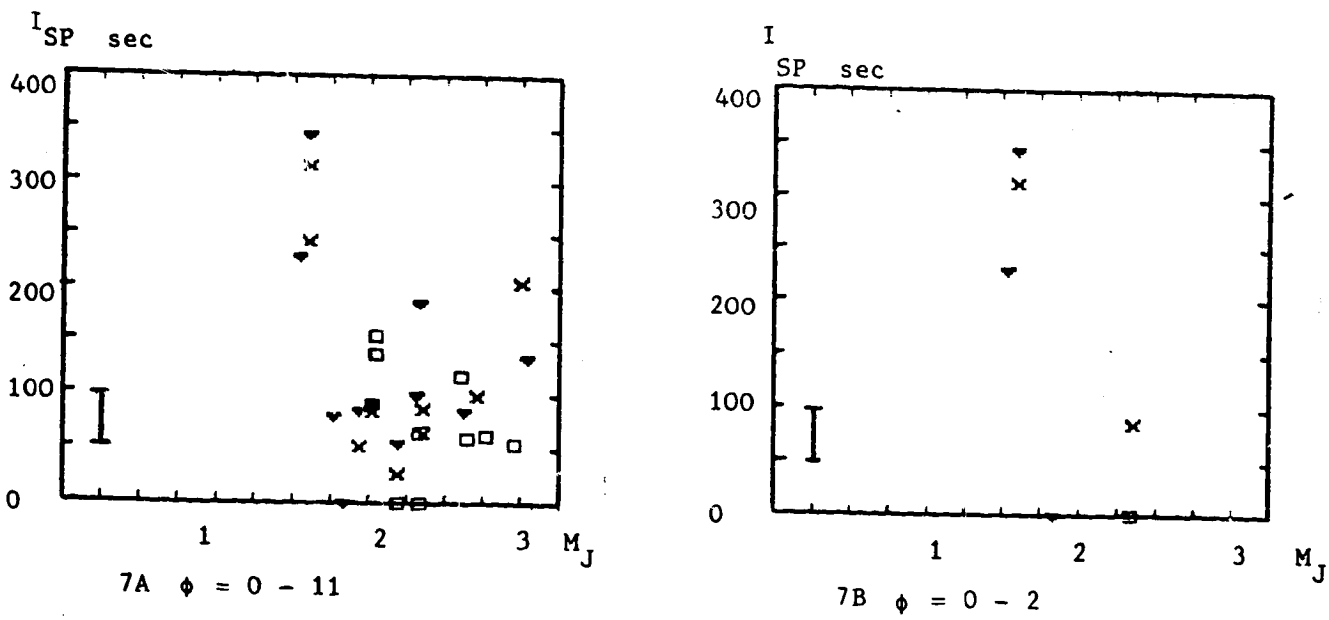

□ H_s = 4.2 × H_s = 6.1 ▼ H_s = 8.7 MJ/kg I error bars

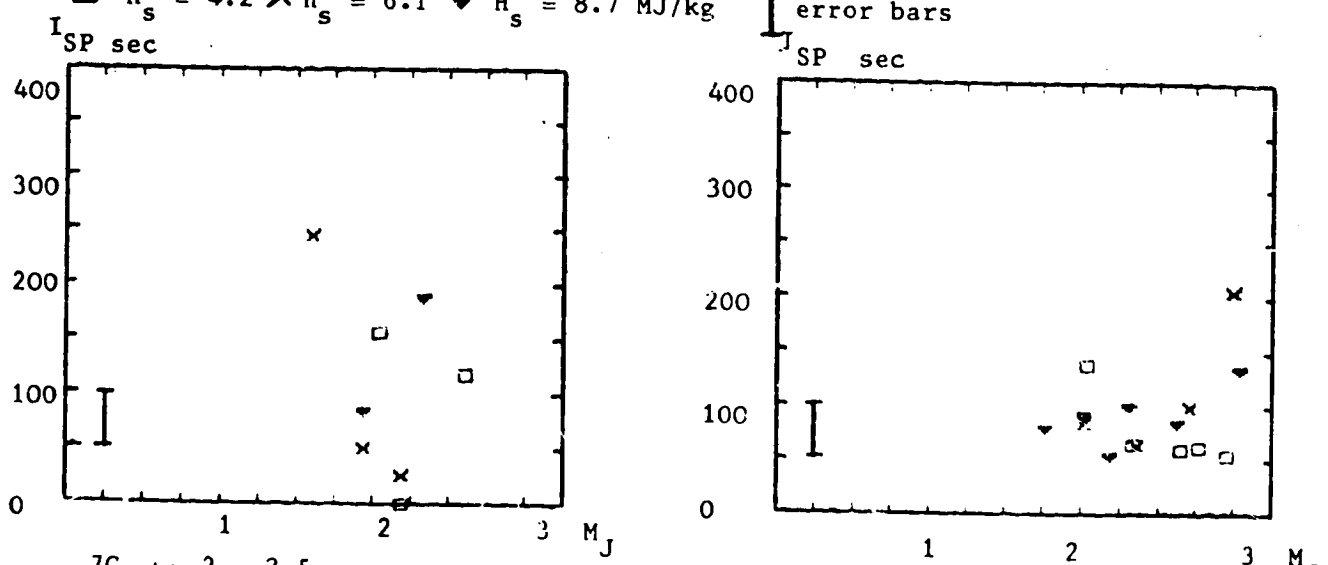

FIG. 7 I_{SP}/M_J 15° diverging duct

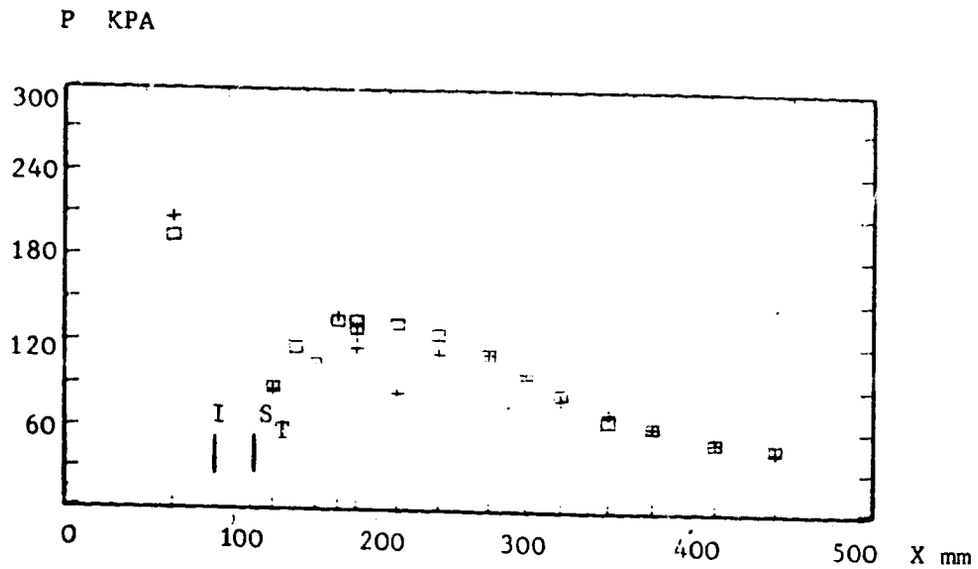

Fig. 8 P/X 15° diverging duct H_S = 8.7 MJ/KG , $\phi \sim 8$

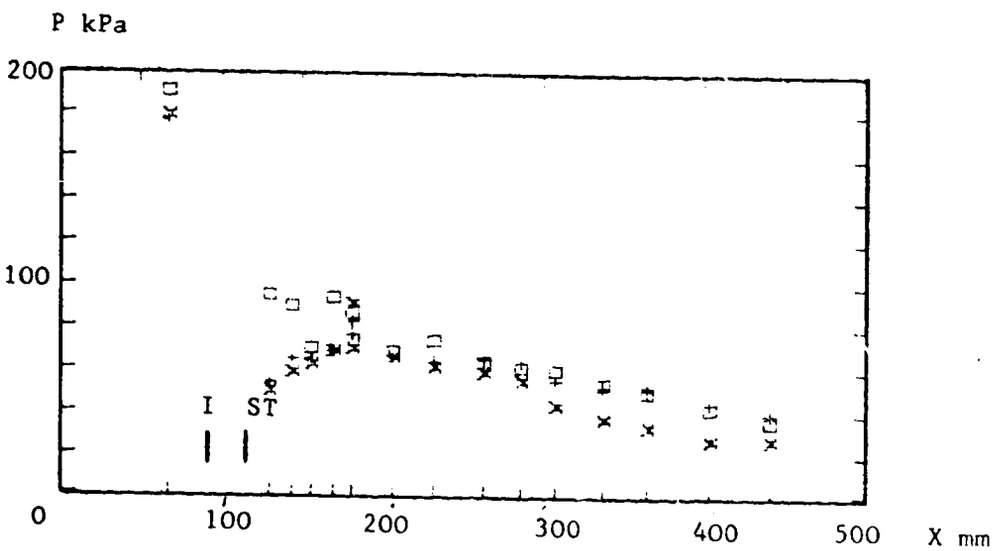

FIG. 9 P/X 15° diverging duct H_s = 6.1 MJ/kg , $\phi \sim 2$

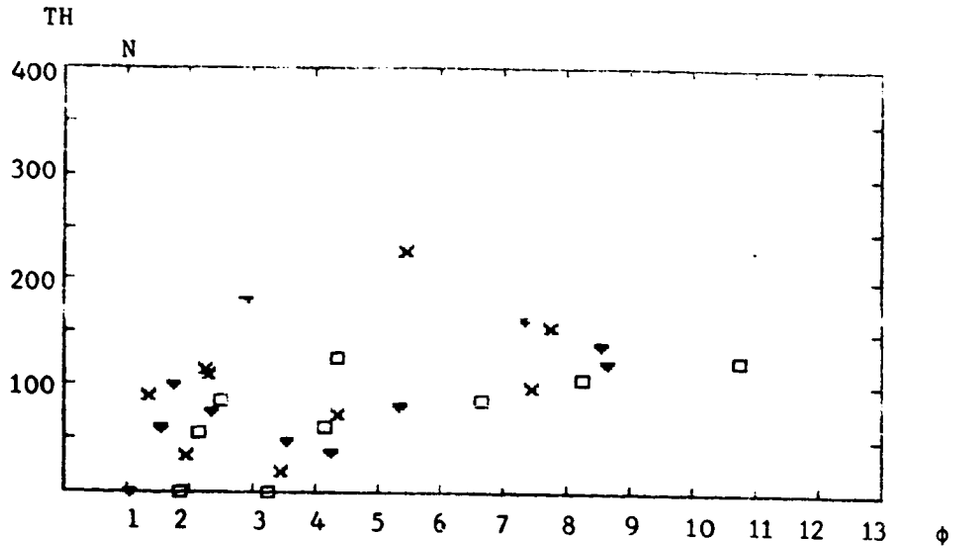

FIG. 10 TH/ϕ 15° diverging duct

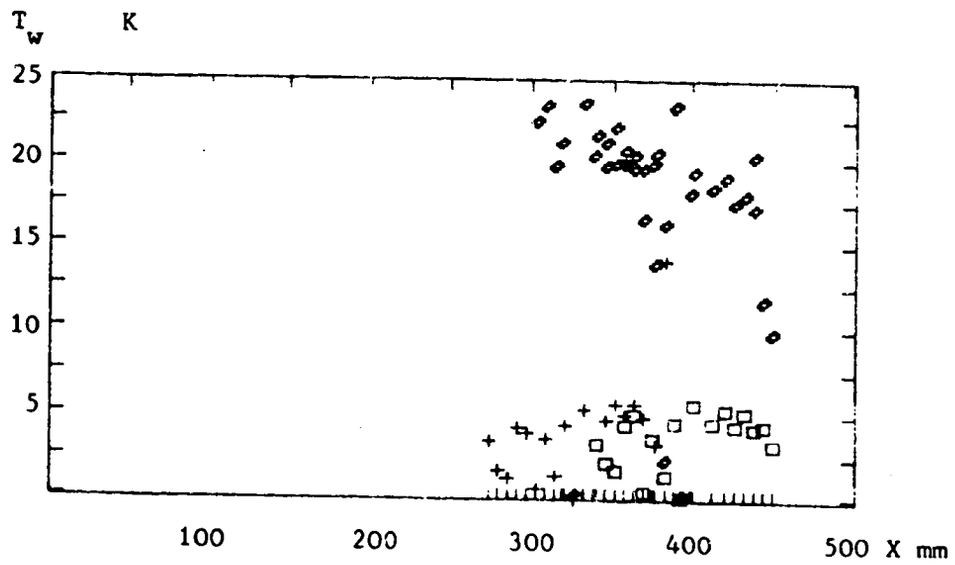

FIG. 11 T_w/X 15° diverging duct, ϕ ~ 8.7 MJ/kg

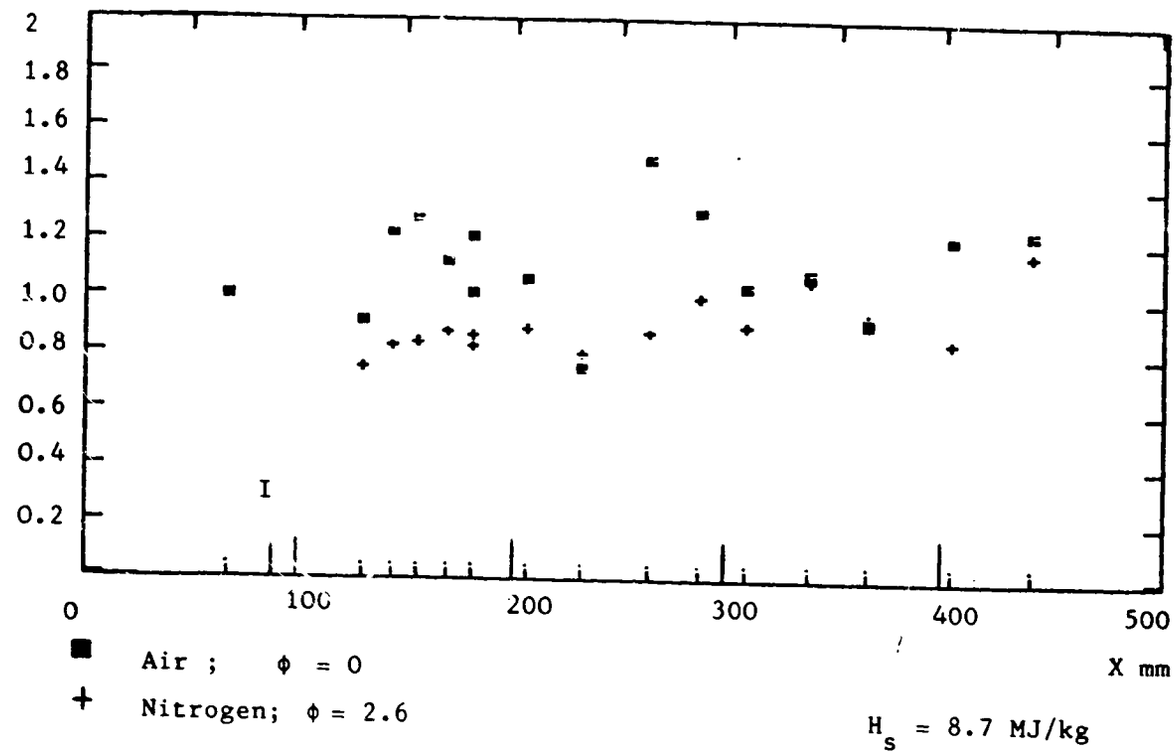

FIG. 12 Pressure profiles in a constant area duct with air and nitrogen test gases.

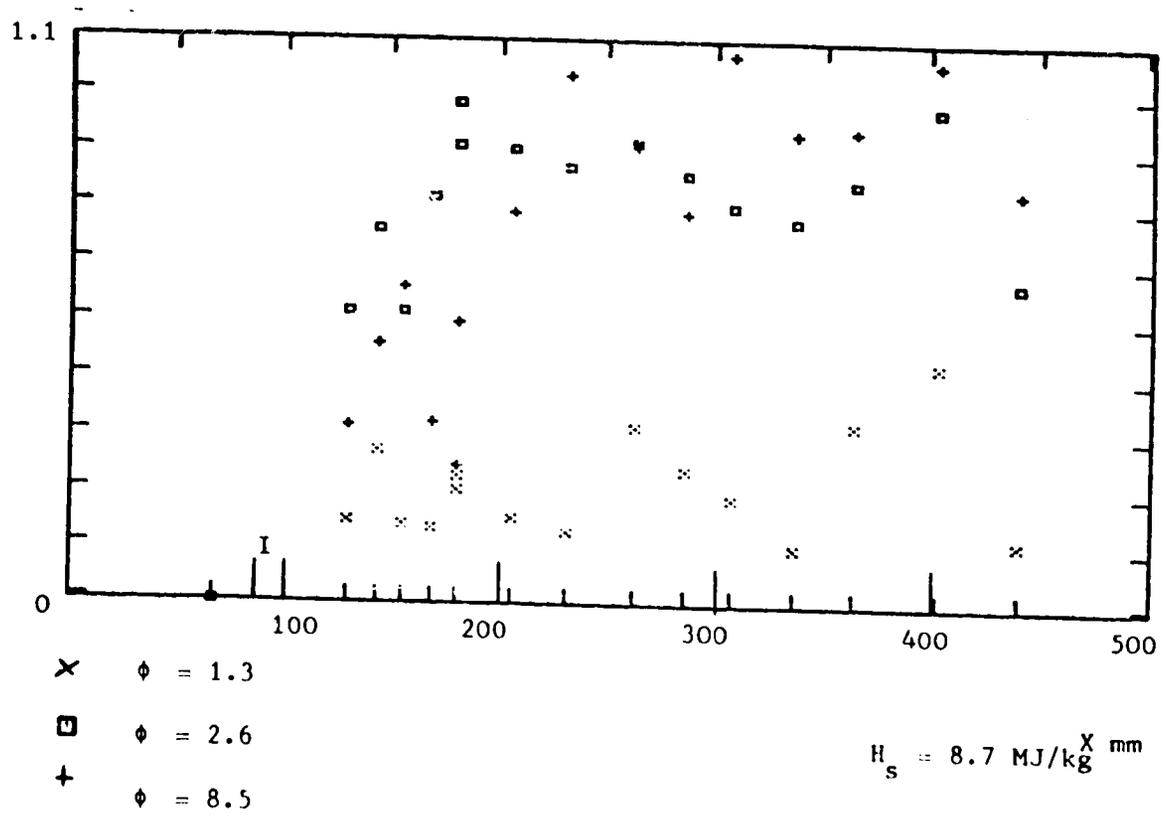

FIG. 13 Pressure profiles in a constant area duct for different equivalence ratios.

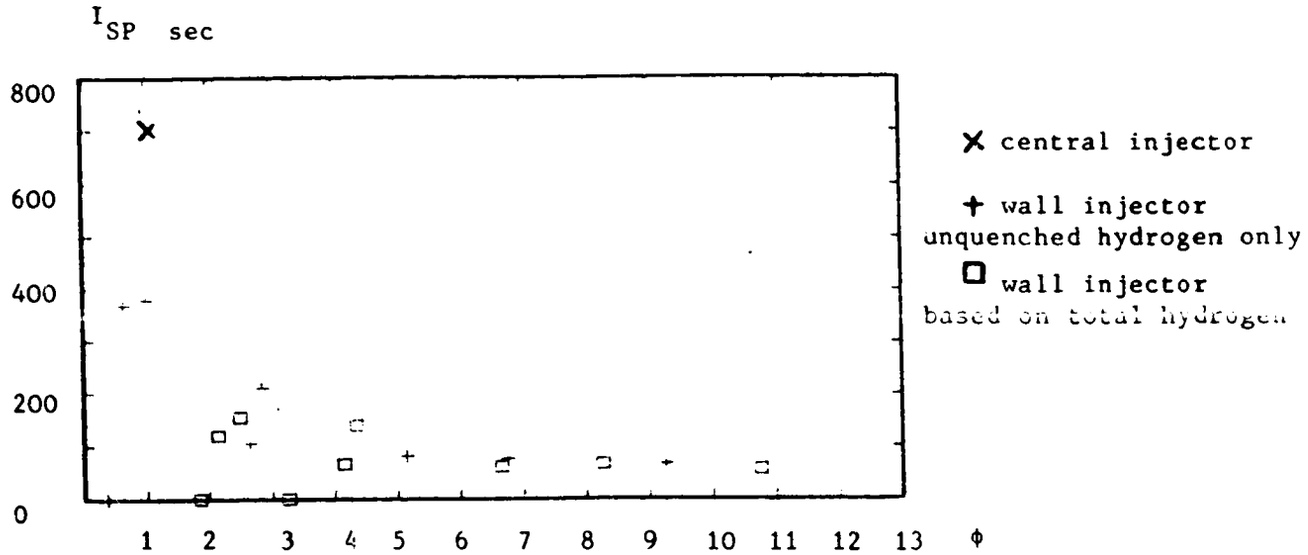

FIG. 14A I_{SP}/ϕ based on quenched and total hydrogen content.

H_s = 4.2 MJ/kg, $\theta_D = 15^o$

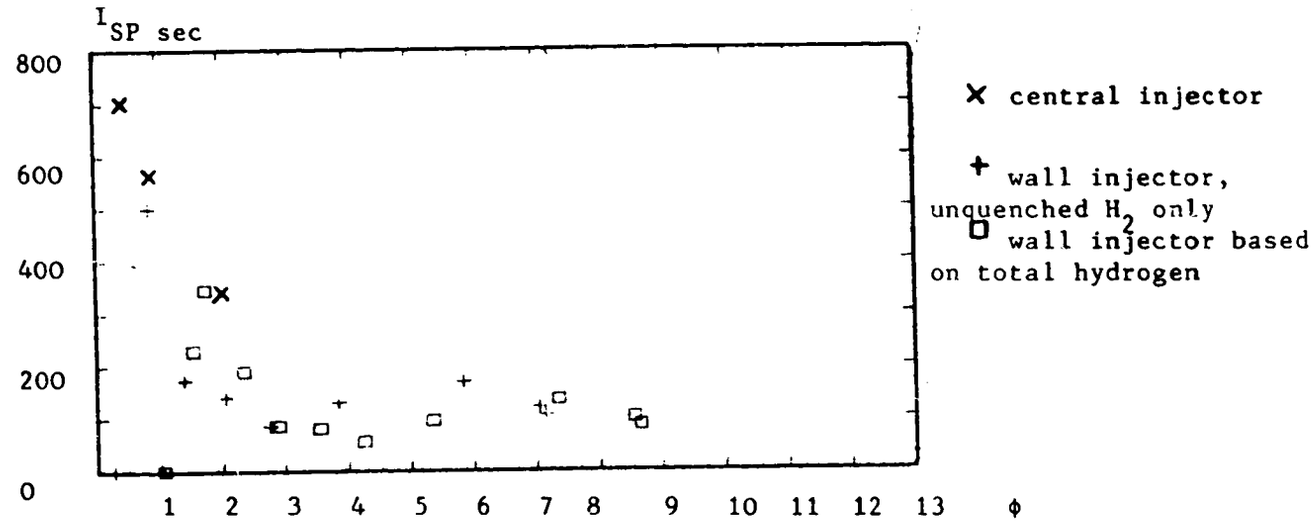

FIG. 14B I_{SP}/ϕ based on quenched and total hydrogen content,

H_s = 8.7 MJ/kg, $\theta_D = 15^o$

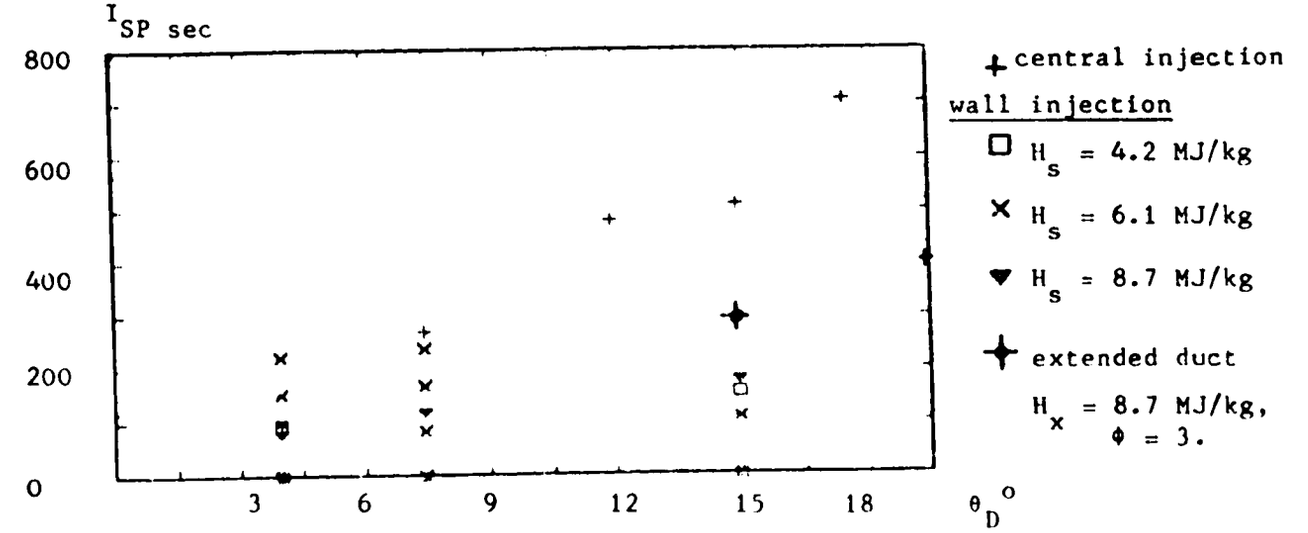

FIG. 15 I_{SP}/θ_D, $\phi \sim 2.5$ wall injection, $\phi = 1$ central injection

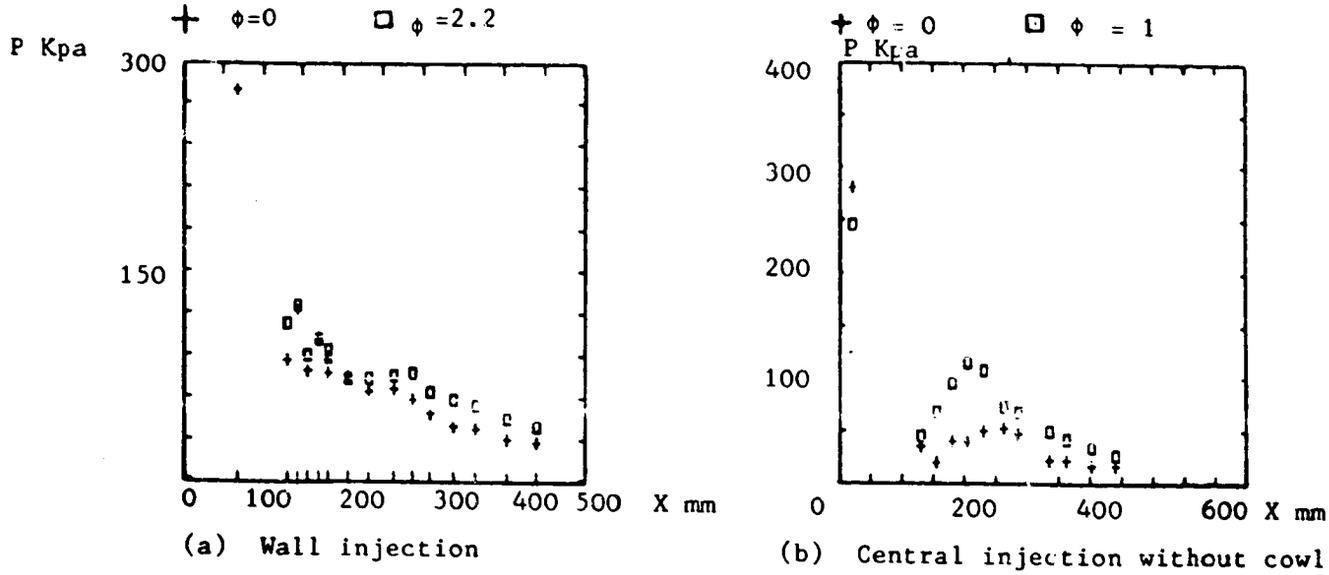

(a) Wall injection (b) Central injection without cowl

FIG. 16 P/X comparison of wall and central injection, H_s = 4.2 MJ/kg

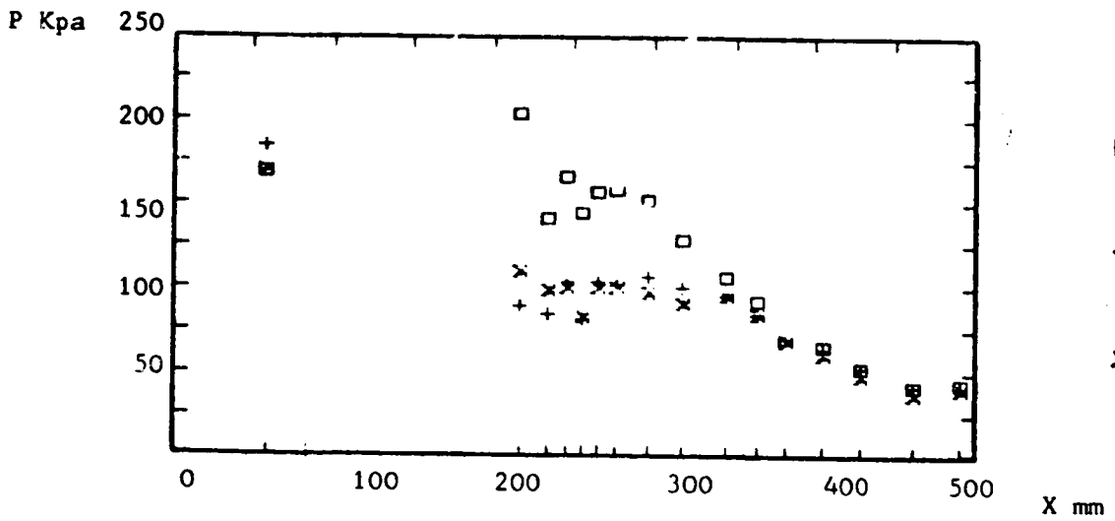

FIG. 17 P/X for extended combustion chamber, $\theta_D = 15^\circ$, H_s = 8.7 MJ/kg

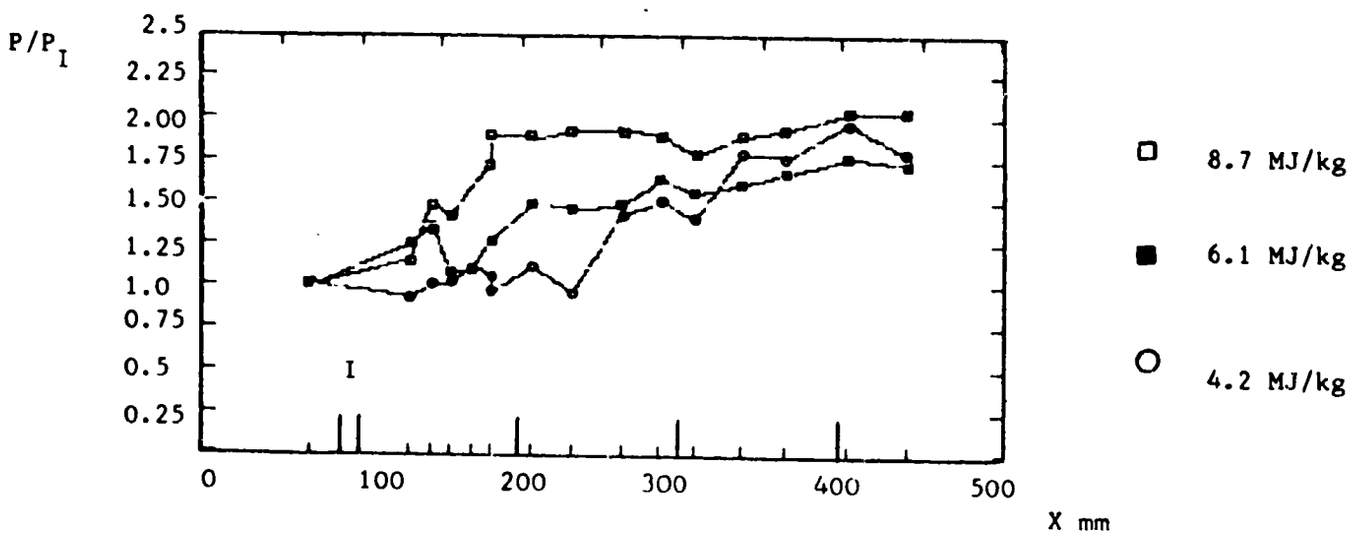

FIG. 18 Pressure profiles for different enthalpies in a constant area duct
ϕ ~ 2.5

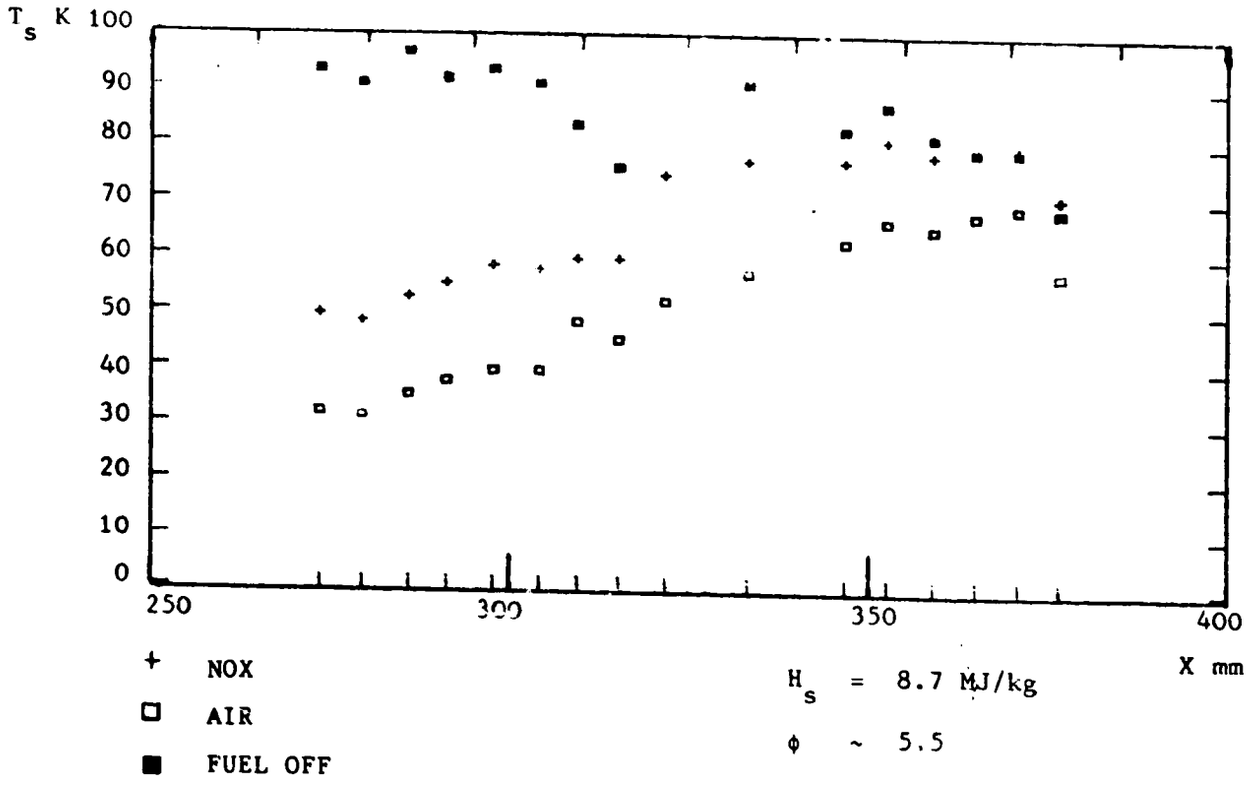

FIG.19 Temperature Profiles for Constant Area Duct NOX and Air Test Gas

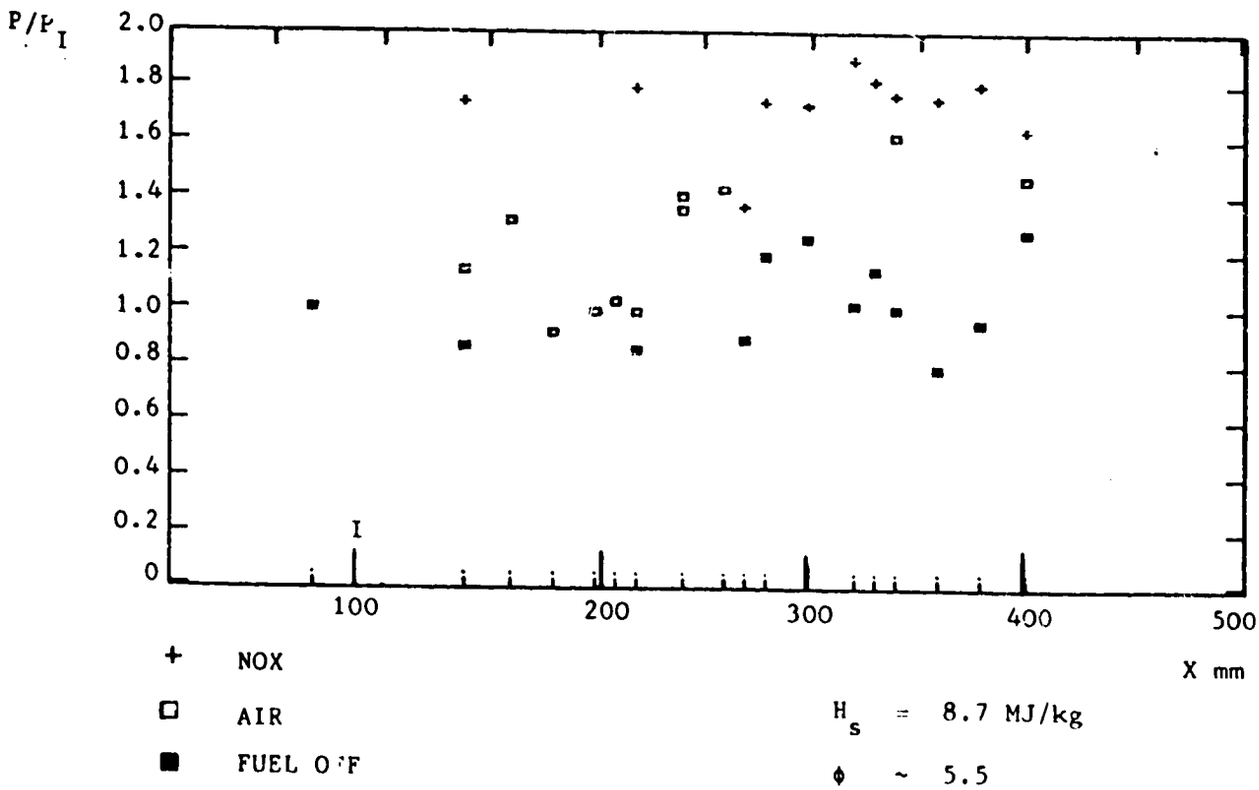

FIG.20 Pressure Profiles for Constant Area Duct, NOX and Air Test Gas

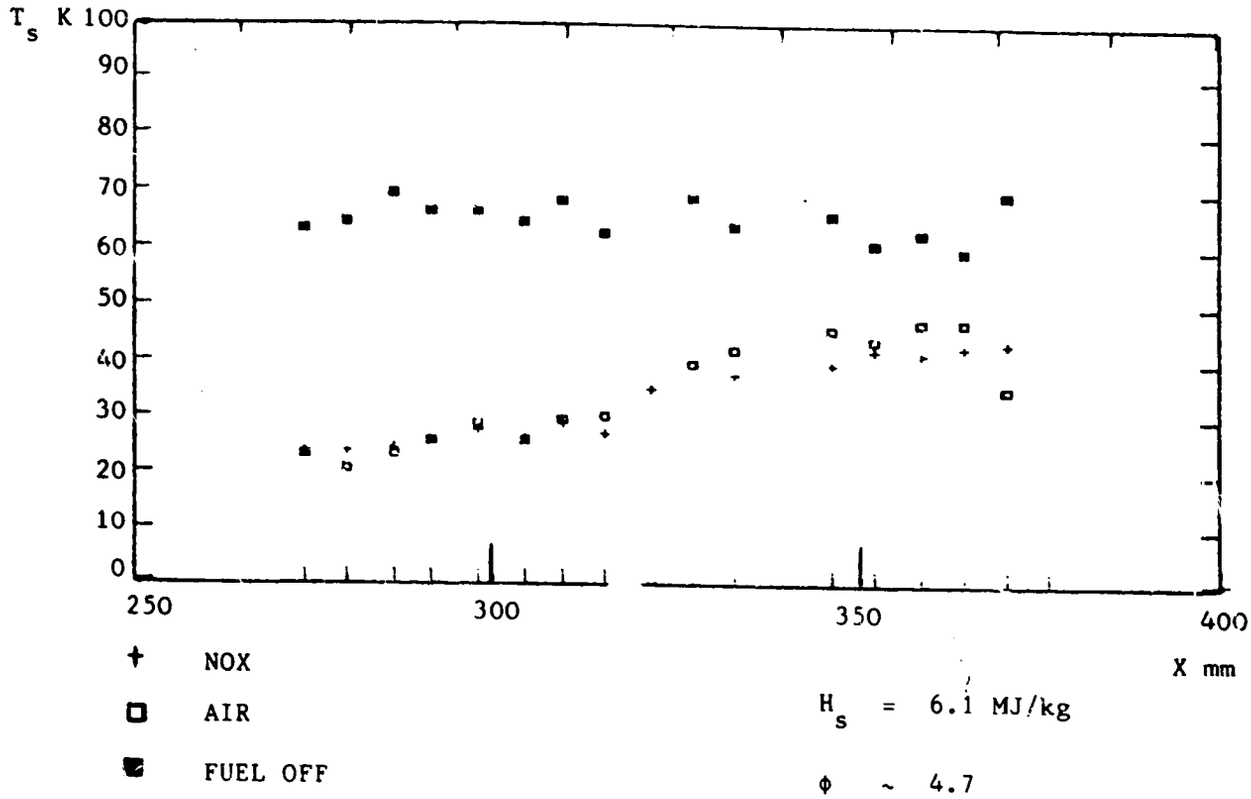

FIG.21 Temperature Profiles for Constant Area Duct, NOX and Air Test Gas

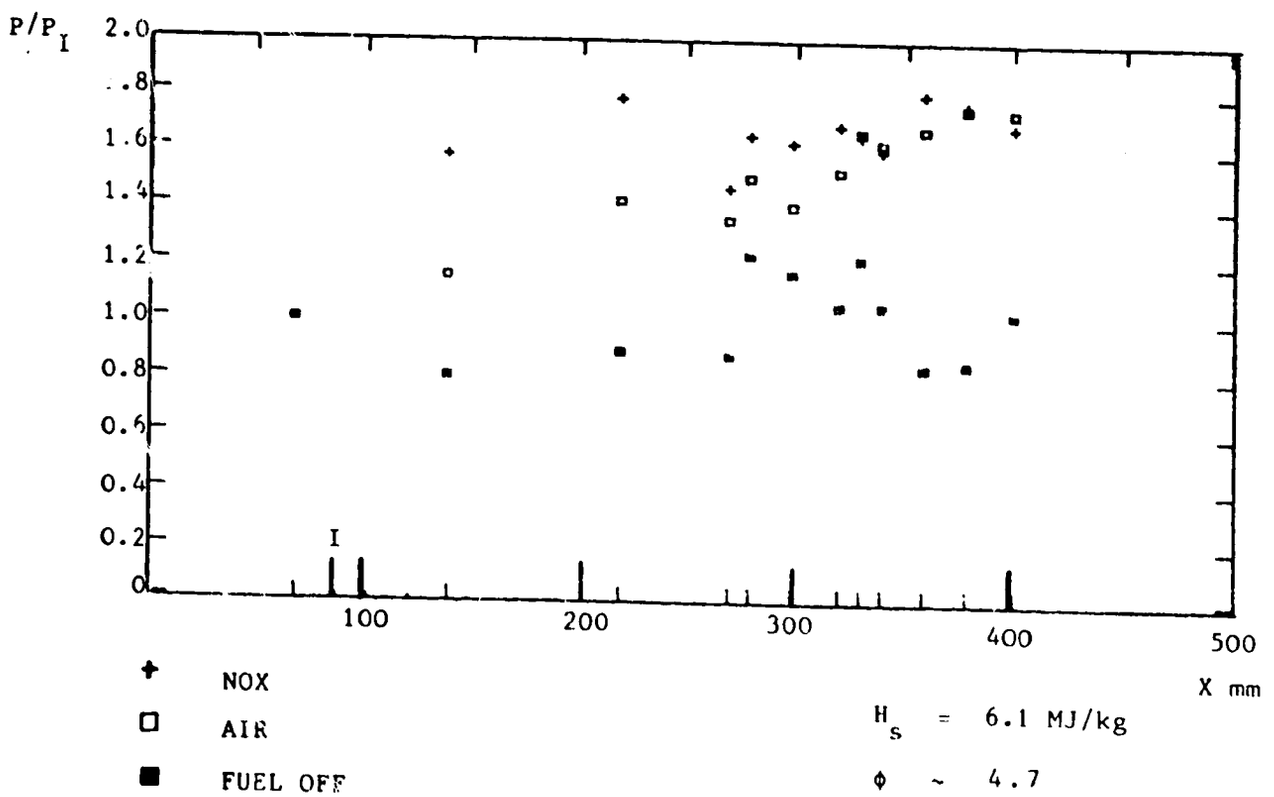

FIG.22 Pressure Profiles for Constant Area Duct, NOX and Air Test Gas

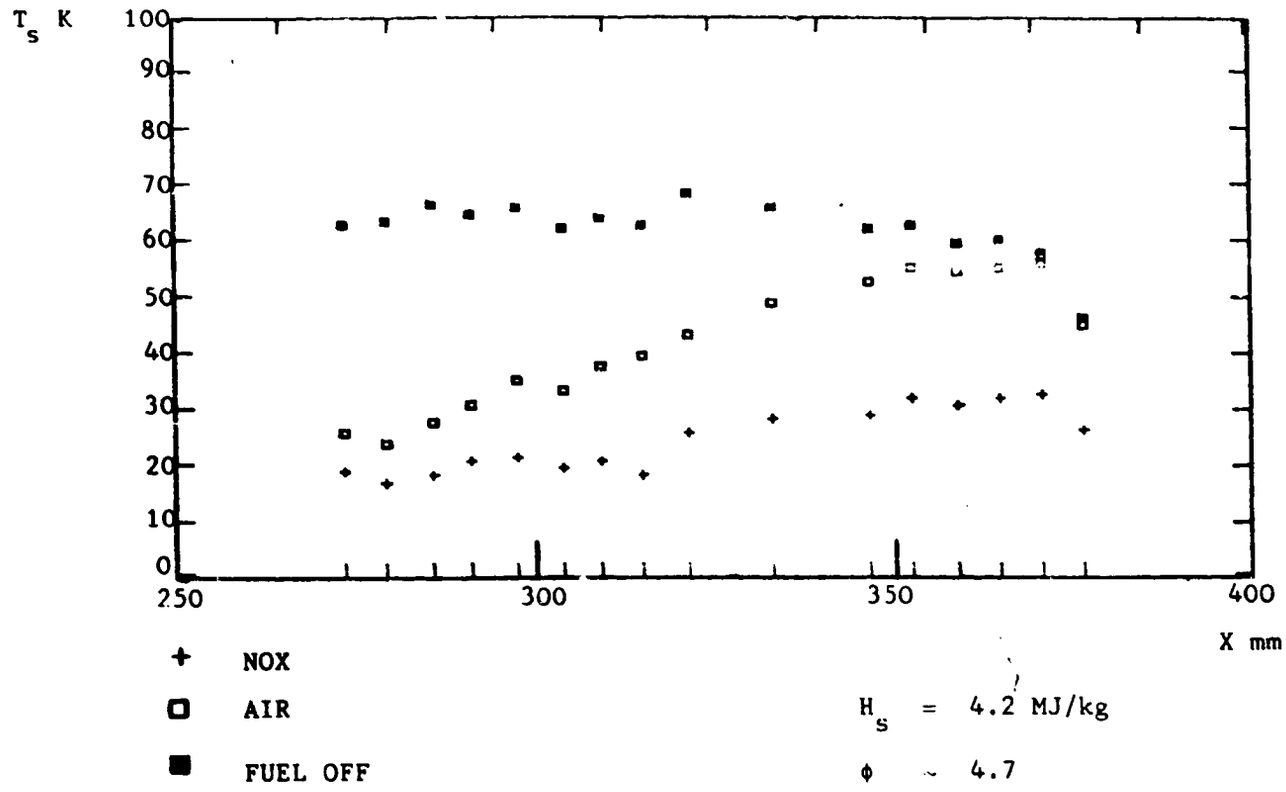

FIG.23 Temperature Profiles for Constant Area Duct, NOX and Air Test Gas

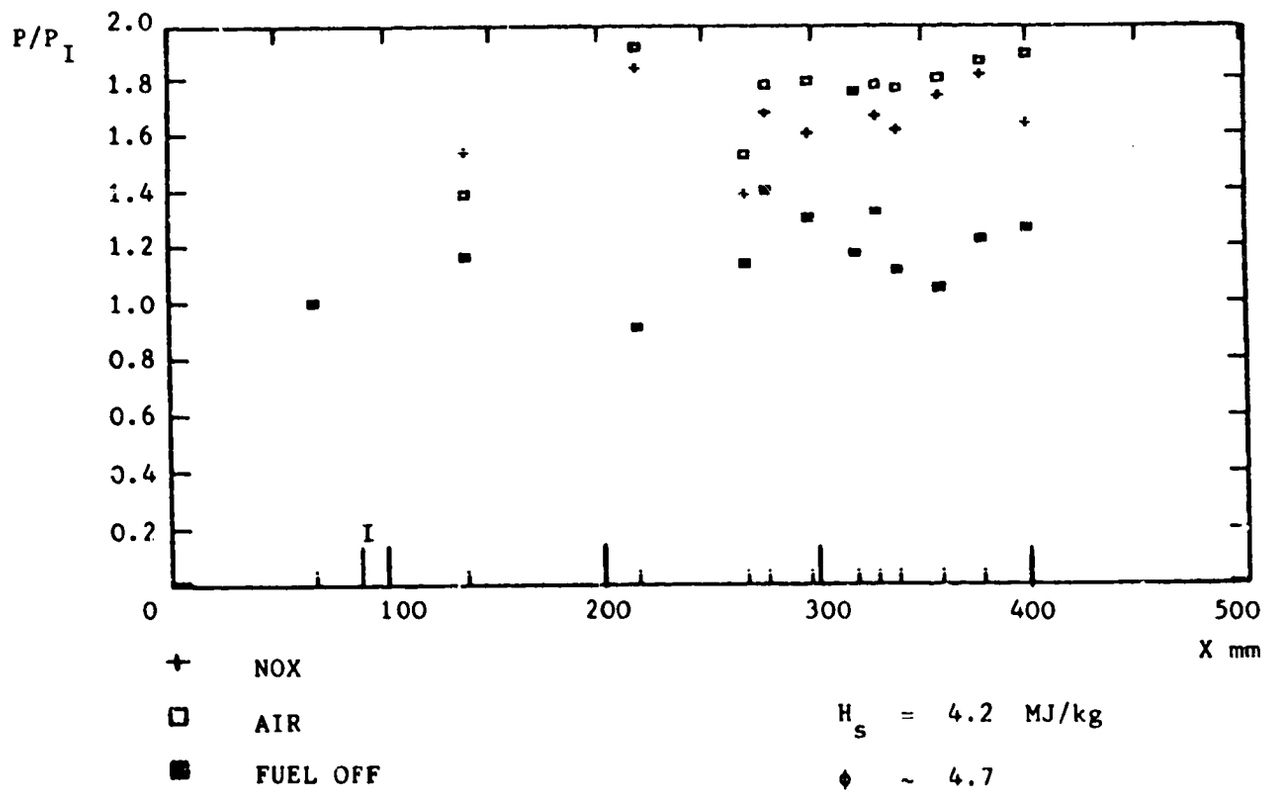

FIG.24 Pressure Profiles for Constant Area Duct, NOX and Air Test Gas

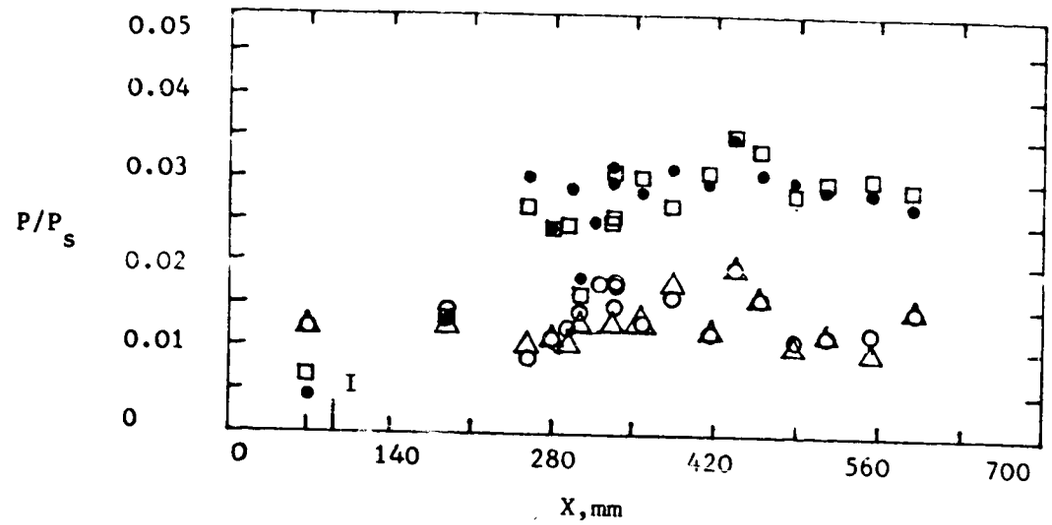

□ H_2 injection, $\phi \sim 1$, H_s = 6.1 MJ/kg

● H_2 injection, $\phi \sim 1$, H_s = 4.2 MJ/kg

○ H_2 injection, $\phi \sim 1$, H_s = 2.65 MJ/kg

△ fuel off, H_s = 2.65 MJ/kg

FIG. 25 Pressure profiles for constant area duct illustrating temperature combustion limit for hydrogen (M_I = 3.5)

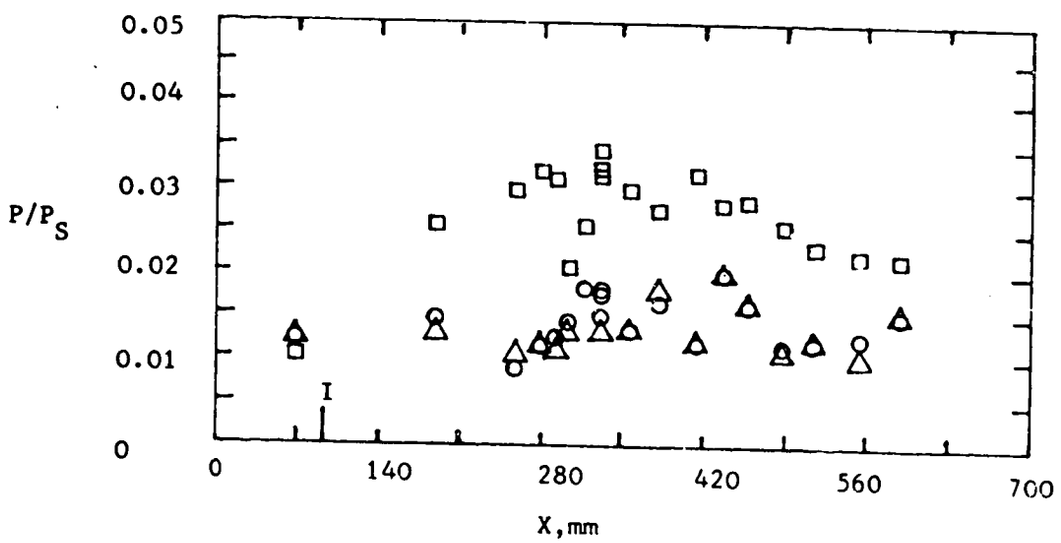

□ Silane injection, $\phi \sim 1$, H_s = 2.65 MJ/kg

○ H_2 injection, $\phi \sim 1$, H_s = 2.65 MJ/kg

△ fuel off, H_s = 2.65 MJ/kg

FIG. 26 Pressure profiles for constant area duct with silane injection at hydrogen combustion limit (M_I = 3.5)

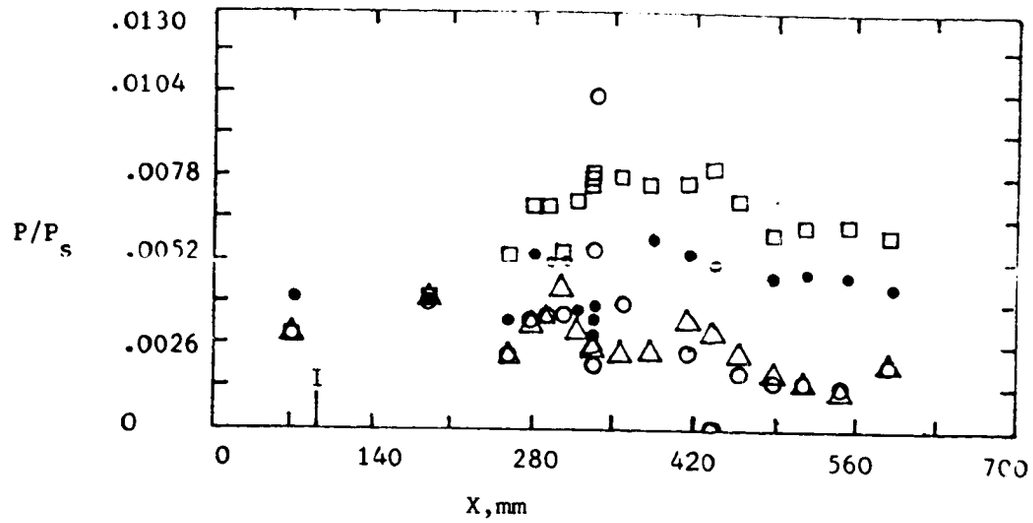

□ H_2 injection, $\phi \sim 1$, H_s = 3.43 MJ/kg

● H_2 injection, $\phi \sim 1$, H_s = 2.65 MJ/kg

○ H_2 injection, $\phi \sim 1$, H_s = 1.90 MJ/kg

△ fuel off, H_s = 1.90 MJ/kg

FIG. 27 Pressure profiles for constant area duct illustrating temperature combustion limit for hydrogen (M_I = 4.5)

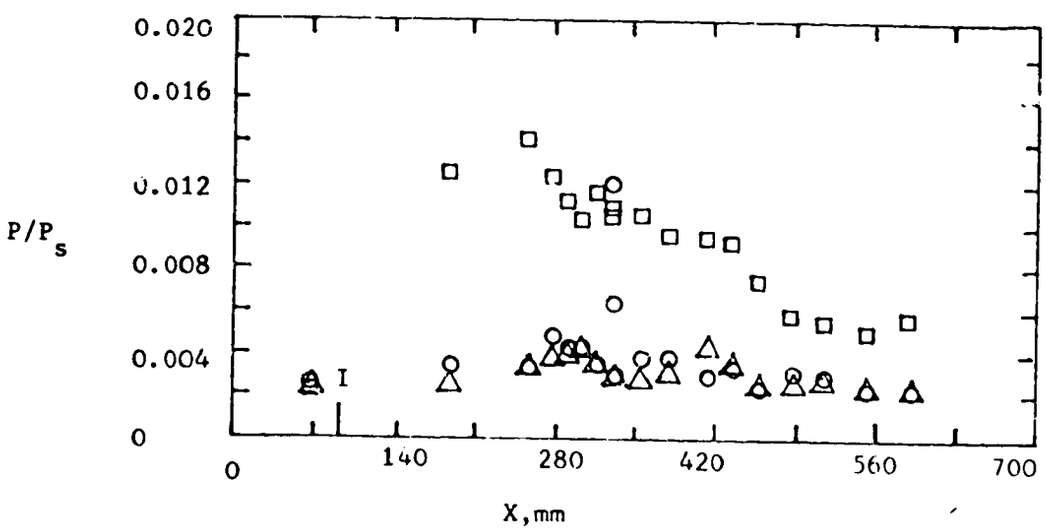

□ Silane injection, $\phi \sim 1$, H_s = 1.90 MJ/kg

○ H_2 injection, $\phi \sim 1$, H_s = 1.90 MJ/kg

△ fuel off, H_s = 1.90 MJ/kg

FIG. 28 Pressure profiles for constant area duct with silane injection at hydrogen combustion limit (M_I = 4.5)

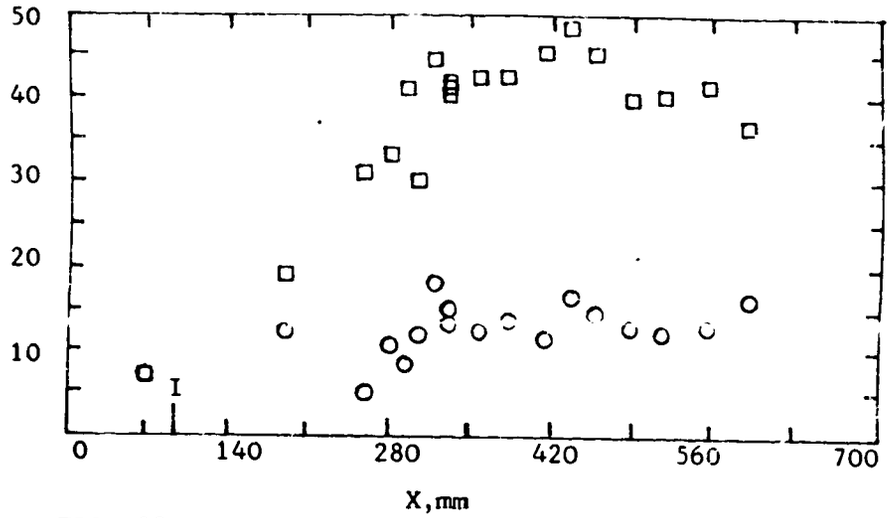

FIG. 29 Pressure profiles for constant area duct with silane injection, $M_I = 5$, $H_s = 4.2$ MJ/kg

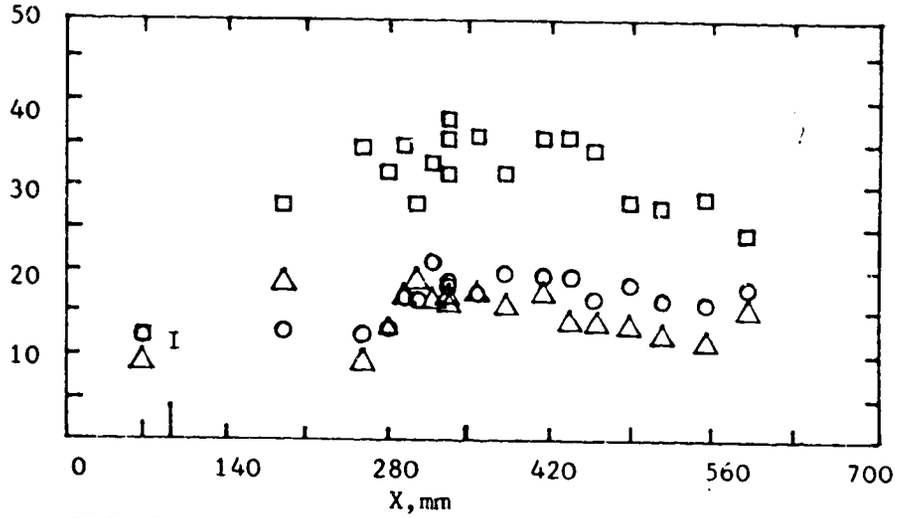

FIG. 30 Pressure profiles for constant area duct with silane injection, $M_I = 5$, $H_s = 6.1$ MJ/kg

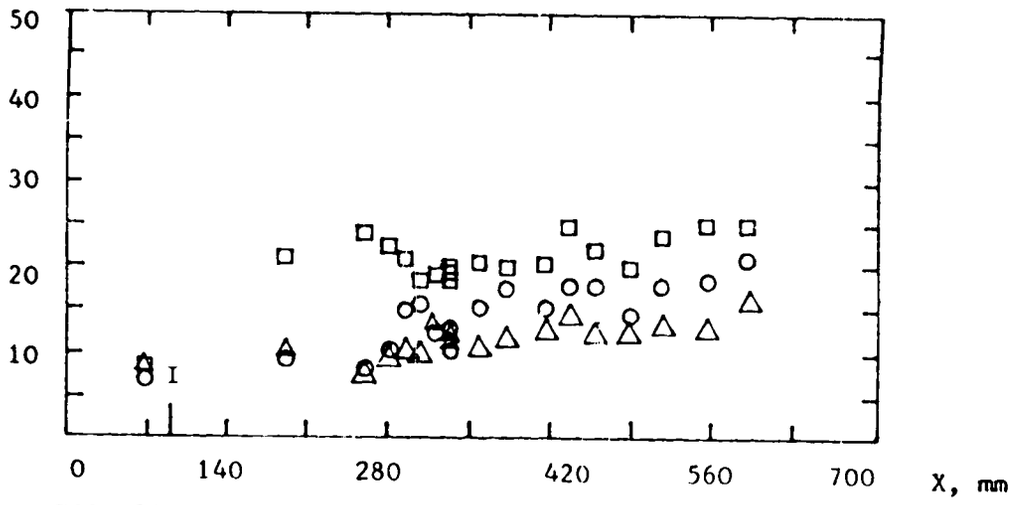

FIG. 31 Pressure profiles for constant area duct with silane injection, $M_I = 5$, $H_s = 8.7$ MJ/kg

SYMBOLS for figures 29, 30, 31	
□	Silane injection, $\phi \sim 1$
○	H_2 injection, $\phi \sim 1$
△	fuel off

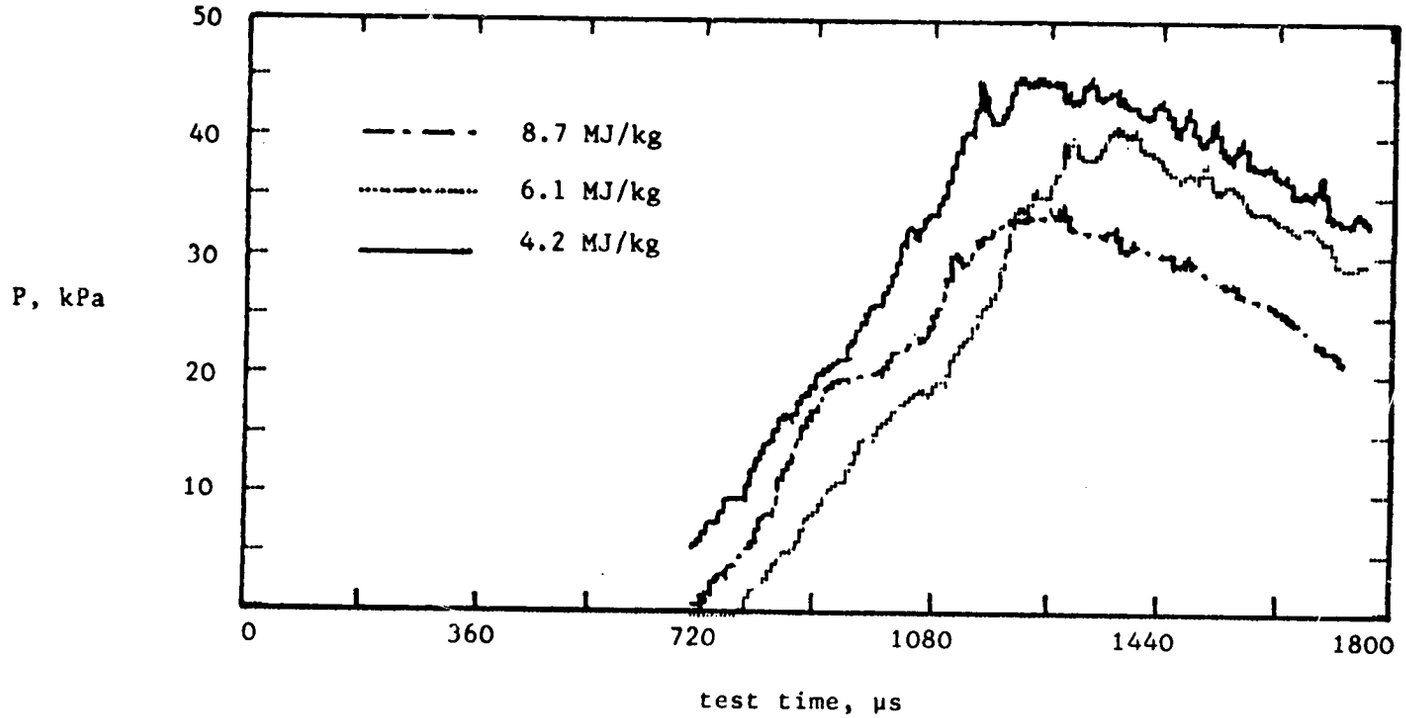

FIG. 32 Average combustion chamber pressure versus test time, constant area duct, silane injection $\phi \sim 1$, $M_I = 5$.

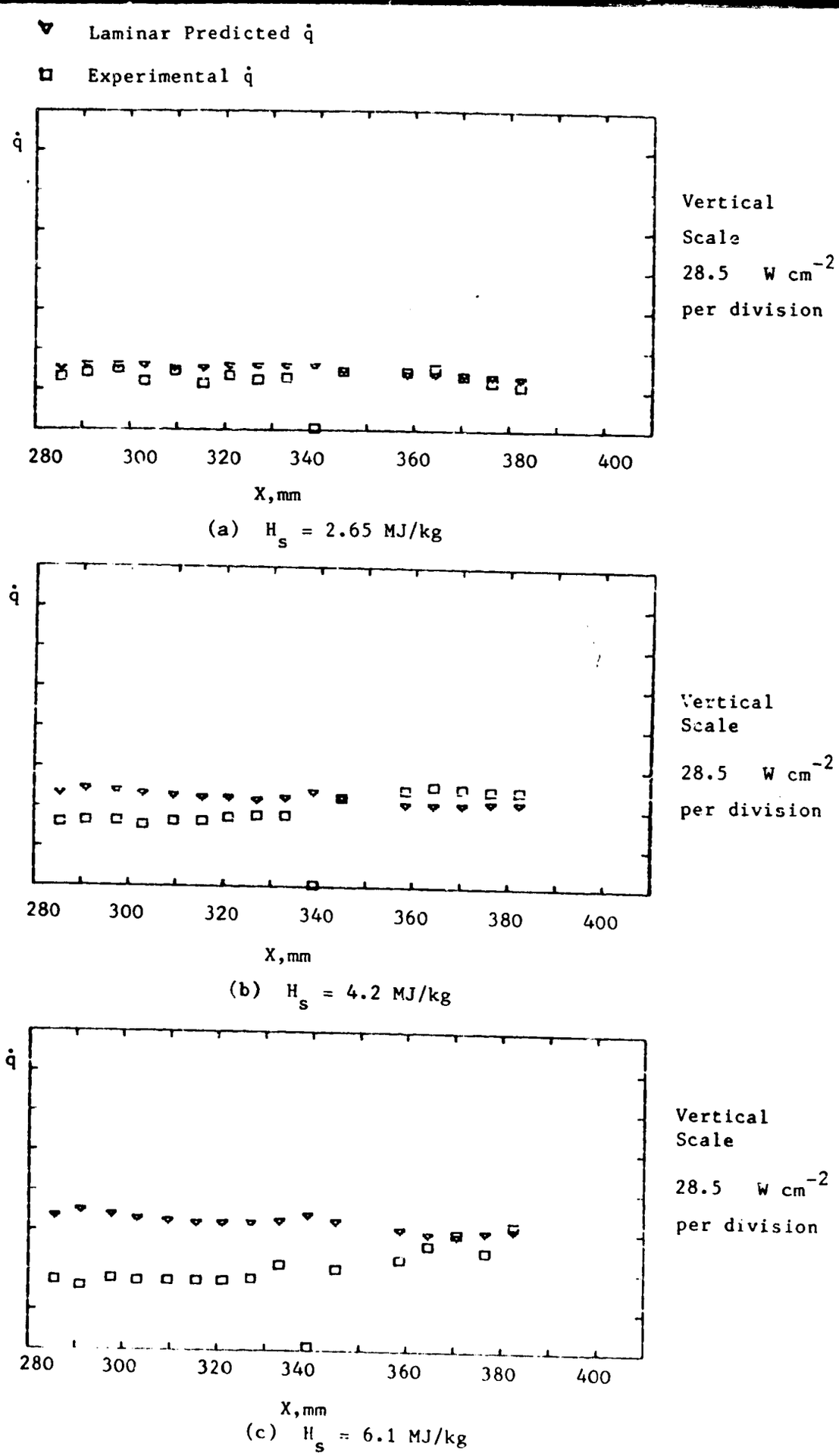

FIG. 33 $\dot{q}$ profiles, constant area duct without injector fitted

M_I = 3.5, Fuel off

▽ Laminar Predicted $\dot{q}$

□ Experimental $\dot{q}$

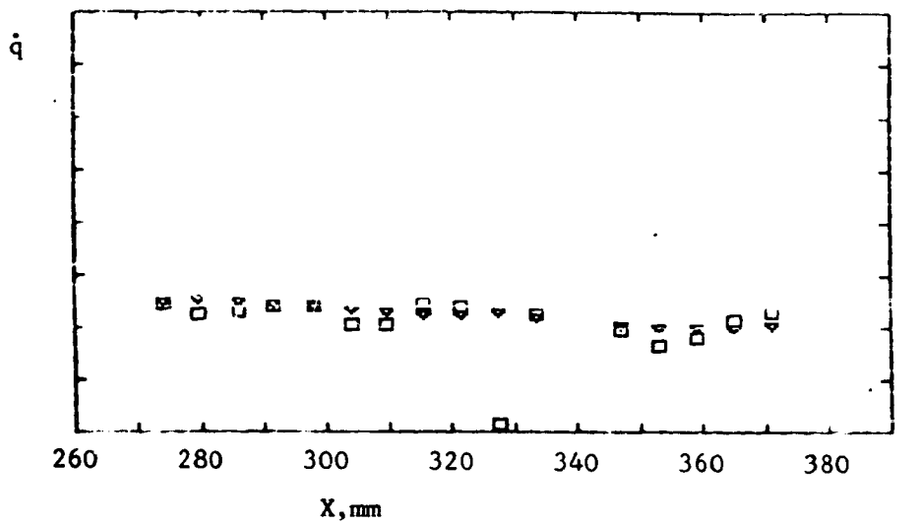

Vertical scale 28.5 W cm^{-2} per division

(a) H_s = 4.2 MJ/kg

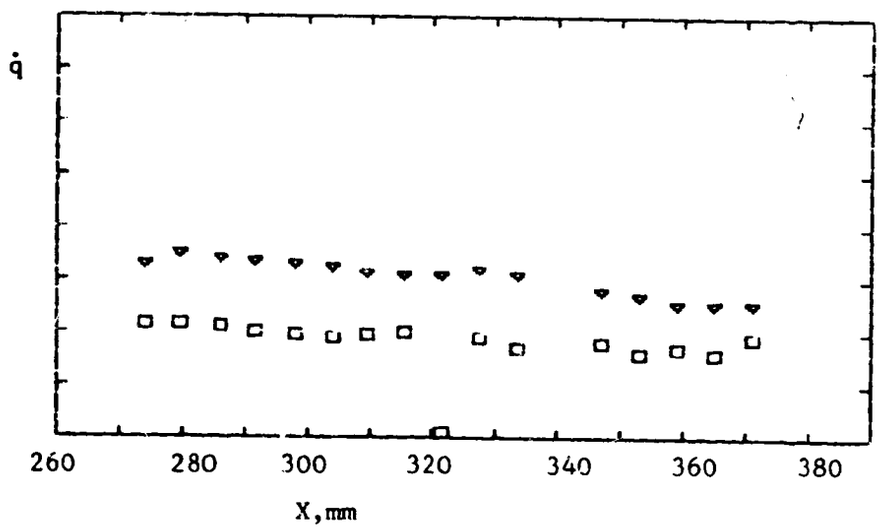

Vertical Scale 28.5 W cm^{-2} per division

(b) H_s = 6.1 MJ/kg

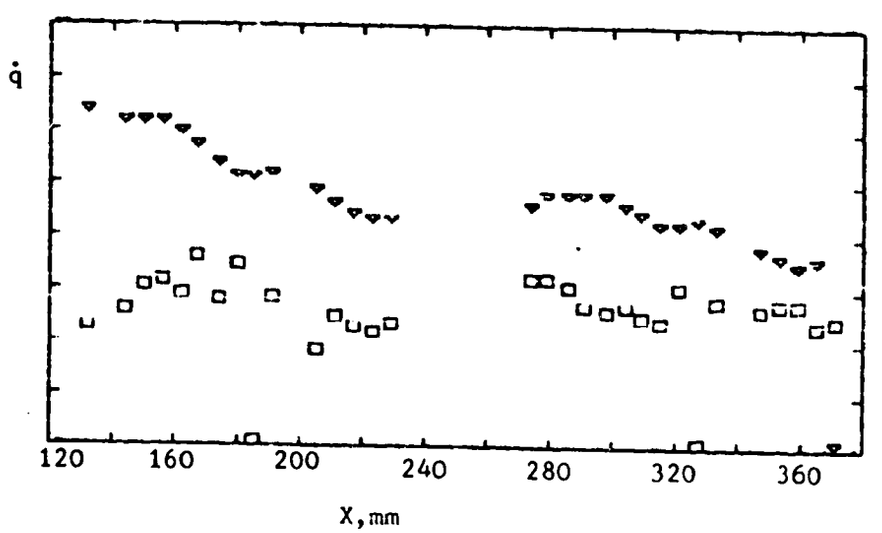

Vertical Scale 28.5 W cm^{-2} per division

(c) H_s = 8.7 MJ/kg

FIG. 34 $\dot{q}$ profiles, Constant area duct with injector fitted, M_I = 3.5, Fuel off

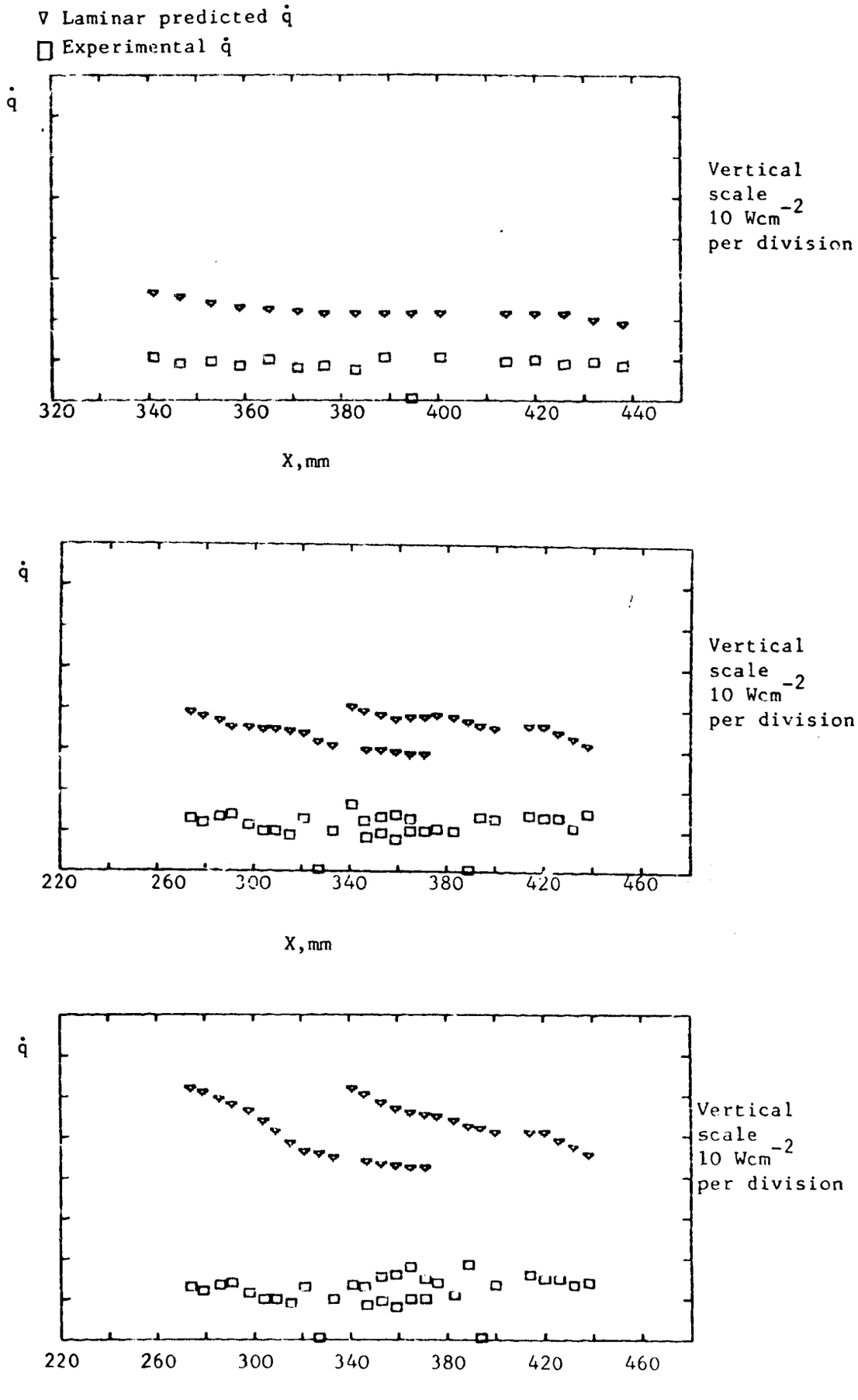

Fig. 35 $\dot{q}$ profiles, 15° diverging duct with wall injector fitted, M_l = 3.5, fuel off.

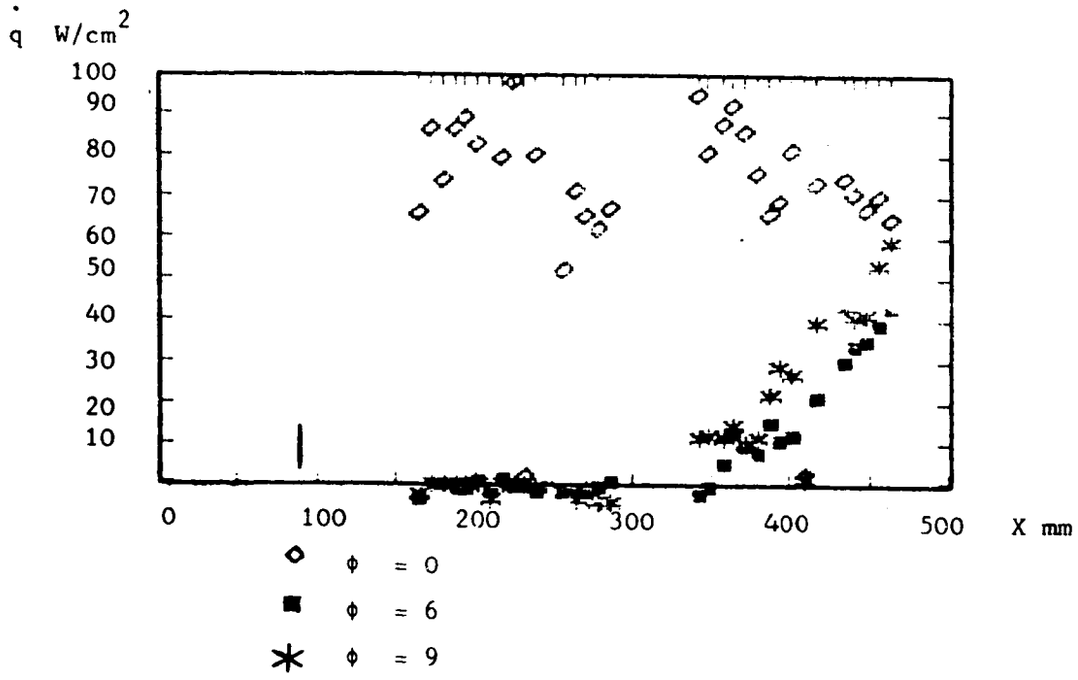

FIG. 36 Constant area duct wall injection of hydrogen. Heat transfer profiles. H_s = 8.7 MJ/kg, M_I = 3.5

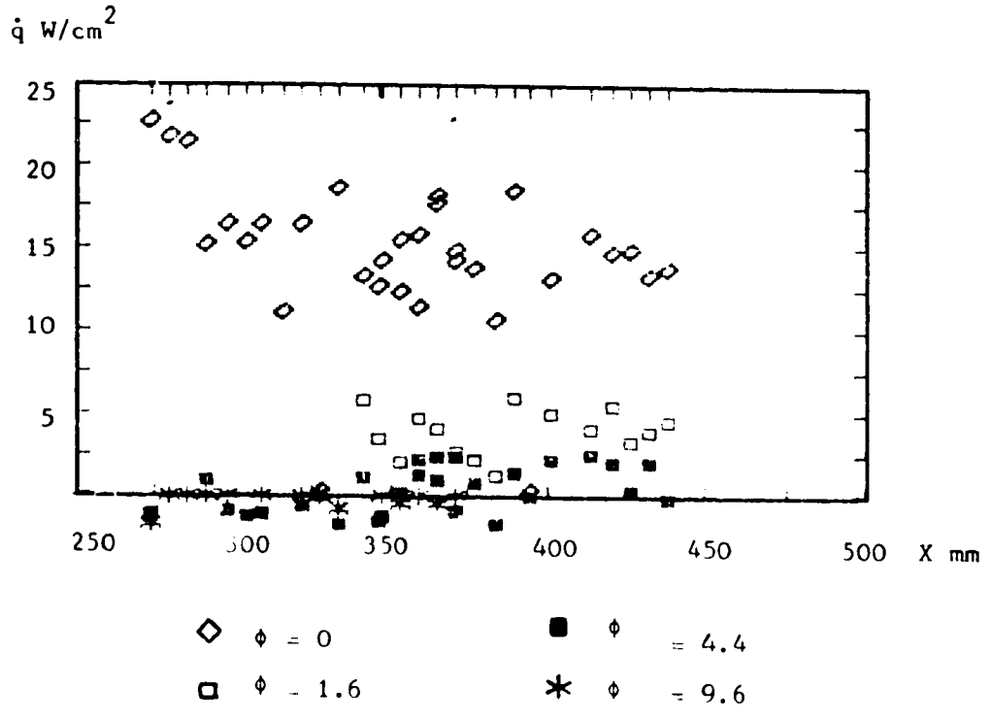

FIG. 37 15° diverging duct wall injection of hydrogen Heat transfer profiles. H_s 8.7 MJ/kgm M_I = 3.5